Monthly Notices
of the
ROYAL ASTRONOMICAL SOCIETY

MNRAS **483,** 5223–5245 (2019)
Advance Access publication 2018 December 10

doi:10.1093/mnras/sty3320

On the lack of correlation between [O III]/[O II] and Lyman continuum escape fraction

R. Bassett,[1,2]★ E. V. Ryan-Weber,[1,2]★ J. Cooke,[1]★ C. G. Diaz ,[3,4,5] T. Nanayakkara,[6] T.-T. Yuan,[1,2] L. R. Spitler,[7,8,9] U. Meštrić,[1,2] T. Garel,[10] M. Sawicki,[11] S. Gwyn[12] and A. Golob[11]

[1]*Centre for Astrophysics and Supercomputing, Swinburne University of Technology, PO Box 218, Hawthorn, VIC 3122, Australia*
[2]*ARC Centre of Excellence for All Sky Astrophysics in 3 Dimensions (ASTRO 3D), Australia*
[3]*Gemini Observatory, Southern Operations Center, Casilla 603, La Serena, Chile*
[4]*Instituto de Ciencias Astronómicas, de la Tierra y del Espacio (ICATE), CP 5400, San Juan, Argentina*
[5]*Consejo de Investigaciones Científicas y Técnicas (CONICET), CABA, Argentina*
[6]*Leiden Observaroty, Leiden University, NL-2300 RA Leiden, the Netherlands*
[7]*Research Centre for Astronomy, Astrophysics & Astrophotonics, Macquarie University, Sydney, NSW 2109, Australia*
[8]*Department of Physics & Astronomy, Macquarie University, Sydney, NSW 2109, Australia*
[9]*Australian Astronomical Observatories, 105 Delhi Rd, Sydney, NSW 2113, Australia*
[10]*Univ Lyon, Univ Lyon1, Ens de Lyon, CNRS, Centre de Recherche Astrophysique de Lyon UMR5574, F-69230 Saint-Genis-Laval, France*
[11]*Department of Astronomy & Astrophysics and the Institute for Computational Astrophysics, Saint Mary's University, Halifax Nova Scotia, B3H 3C3, Canada*
[12]*NRC-Hertzberg, 5071 West Saanich Road, VIC, BC V9E 2E7, Canada*

Accepted 2018 November 27. Received 2018 November 18; in original form 2018 April 10

ABSTRACT

We present the first results of our pilot study of eight photometrically selected Lyman-continuum (LyC) emitting galaxy candidates from the COSMOS field and focus on their optical emission line ratios. Observations were performed in the H and K bands using the Multi-Object Spectrometer for Infra-Red Exploration (MOSFIRE) instrument at the Keck Observatory, targeting the [O II], H β, and [O III] emission lines. We find that photometrically selected LyC emitting galaxy candidates have high ionization parameters, based on their high [O III]/[O II] ratios (O32), with an average ratio for our sample of 2.5 ± 0.2. Preliminary results of our companion Low-Resolution Imaging Spectrometer (LRIS) observations, targeting LyC and Ly α, show that those galaxies with the largest O32 are typically found to also be Ly α emitters. High O32 galaxies are also found to have tentative non-zero LyC escape fractions ($f_{\rm esc}$(LyC)) based on u band photometric detections. These results are consistent with samples of highly ionized galaxies, including confirmed LyC emitting galaxies from the literature. We also perform a detailed comparison between the observed emission line ratios and simulated line ratios from density bounded H II regions modelled using the photoionization code MAPPINGS V. Estimates of $f_{\rm esc}$(LyC) for our sample fall in the range from 0.0 to 0.23 and suggest possible tension with published correlations between O32 and $f_{\rm esc}$(LyC), adding weight to dichotomy of arguments in the literature. We highlight the possible effects of clumpy geometry and mergers that may account for such tension.

Key words: galaxies: intergalactic medium – galaxies: ISM – cosmology: dark ages, reionization, first stars.

1 INTRODUCTION

The epoch of reionization (EoR) is a fundamental cosmological event marking a phase shift of the intergalactic medium (IGM) from neutral to ionized. In the past few decades, a major effort has been put in by the astronomical community into understanding what drives this shift and how the process of reionization proceeds.

★ E-mail: rbassett@swin.edu.au (RB); eryanweber@swin.edu.au (EVR-W); jeffreycooke@swin.edu.au (JC)

Although fairly tight constraints have been placed on the redshift marking the end of the EoR around $z = 6$ (Fan, Carilli & Keating 2006; Komatsu et al. 2011; Zahn et al. 2012; Becker et al. 2015), important open questions remain. In particular, the identity and precise nature of the sources of the required ionizing radiation are uncertain.

It appears likely that the main source of ionizing photons must be hosted by galaxies: either massive stars in rapidly star-forming regions, or quasars (QSOs). There is mounting evidence for a rapid drop in the number density of QSOs above $z = 6$ suggesting that these objects do not represent the main drivers of reionization (Hopkins, Richards & Hernquist 2007; Jiang et al. 2008; Fontanot, Cristiani & Vanzella 2012; Masters et al. 2012; Mitra, Ferrara & Choudhury 2013; Ueda et al. 2014; McGreer et al. 2017; Hassan et al. 2018). This observation has compelled researchers studying the EoR to focus instead on young, star-forming galaxies (Ouchi et al. 2009; Wise & Cen 2009; Yajima, Choi & Nagamine 2011; Bouwens et al. 2015; Paardekooper, Khochfar & Dalla Vecchia 2015). In such galaxies, high-energy stars (O/B stars, Wolf-Rayet stars, and/or X-ray binaries) represent the primary sources of ionizing photons (Rauw et al. 2015; Eldridge et al. 2017). One crucial unknown regarding star-forming galaxies during the EoR, however, is: what are the conditions that allow high-energy photons to escape from galaxies and subsequently ionize the IGM?

A key quantity in this framework is the fraction of ionizing, Lyman continuum photons (LyC, $\lambda < 912$ Å) that escape from star-forming galaxies into the IGM, $f_{\rm esc}$(LyC). Observation of LyC photons is difficult, however, due to a combination of factors both internal and external to the source galaxy. Studies of galaxies during the EoR predict that an average $f_{\rm esc}$(LyC) of ∼0.10–0.20 is required to drive reionization (Ouchi et al. 2009; Raičević, Theuns & Lacey 2011; Fontanot et al. 2012; Robertson et al. 2013; Dressler et al. 2015). Although hydrodynamical simulations show that LyC escape fraction can reach up to 1.0 in some cases (though only briefly, e.g. Trebitsch et al. 2017; Rosdahl et al. 2018), from observations the majority of confirmed Lyman continuum emitting galaxies (LCEs) have $f_{\rm esc}$(LyC) estimates below 0.15 (Leitet et al. 2013; Borthakur et al. 2014; Izotov et al. 2016; Leitherer et al. 2016). There are a few examples of galaxies with estimated $f_{\rm esc}$(LyC) as high as 0.45-0.73 (Bian et al. 2017; Vanzella et al. 2017; de Barros et al. 2016; Shapley et al. 2016; Vanzella et al. 2016; Fletcher et al. 2018 Izotov et al. 2018b,a), however these galaxies are extremely rare. This paucity of examples of high $f_{\rm esc}$(LyC) galaxies is consistent with the brevity of a high $f_{\rm esc}$(LyC) phase seen in simulations, however a lack of large observational samples makes quantifying the relative contribution from star-forming galaxies to reionization challenging.

A related issue, and another contributor to the scarcity of observed strong LCEs, is the opacity of the IGM to ionizing photons. Neutral IGM gas can attenuate, or even absorb completely, LyC photons that escape from galaxies. Prior to and during the EoR, the IGM is mostly neutral and opaque to ionizing photons (Inoue et al. 2014; Grazian et al. 2016). Coupled with the faintness of high-redshift galaxies, this means that escaping LyC photons from the galaxies that actually drive reionization (i.e. galaxies at $z \gtrsim 6.0$) are highly unlikely to be observed. Thus, quantifying $f_{\rm esc}$(LyC) during the EoR will require a proxy for LyC escape that is more readily observed during this epoch. In this vein, on-going projects focus on identifying large samples of post-EoR LCEs and targeting these galaxies at wavelengths longer than LyC in search of other galaxy properties that are correlated with $f_{\rm esc}$(LyC) (e.g. Izotov et al. 2016, 2018b).

An example of a proxy for $f_{\rm esc}$(LyC) that has been under recent scrutiny is the ratio of [O III] (λ5007 Å) to [O II] (λλ3272 Å)(the O32 ratio, e.g. Nakajima & Ouchi 2014). From photoionization modelling, it has been shown that, in H II regions with ionization-bounded conditions (i.e. $f_{\rm esc}$(LyC) = 0), a value of O32 $\gtrsim 1$ is related to high ionization (i.e. a 'hard' ionizing spectrum, Kewley & Dopita 2002; Martín-Manjón et al. 2010). Alternatively, O32 will also increase in density-bounded H II regions or in clumpy star-forming regions where channels for LyC escape represent 'holes' into the hot, higher ionization, [O III] (λ5007 Å) emitting inner regions of nebulae that bypass cooler, low ionization, [O II] (λλ3727 Å) emitting outer regions (Giammanco, Beckman & Cedrés 2005; Pellegrini et al. 2012; Jaskot & Oey 2013; Zackrisson, Inoue & Jensen 2013; Zackrisson et al. 2017). In such a scenario, galaxies with larger O32 ratios would contain H II regions having a larger fraction of their surfaces exhibiting conditions susceptible to LyC escape.

Indeed, Izotov et al. (2018b) has shown that low-redshift LCEs are found to have O32 ratios > 5, and that O32 appears to correlate with $f_{\rm esc}$(LyC). Furthermore, Ion2 (de Barros et al. 2016), the one example of a high-LCE also having measured fluxes of [O III] (λ5007 Å) and [O II] (λλ3727 Å), has an $f_{\rm esc}$(LyC) and O32 similar to the strongest low-redshift LCE from Izotov et al. (2018b). Whether or not the O32 ratio has a direct correlation with $f_{\rm esc}$(LyC) is still a matter of debate, although recent results refute such a strong relationship (Izotov et al. 2018a; Naidu et al. 2018). What remains to be done is to greatly increase the samples of LCE at both low- and high-redshift in order to conclusively test the relationship between $f_{\rm esc}$(LyC) and the O32 ratio.

In this paper, we present the optical line ratios, including O32, for a pilot sample of galaxies selected as LCE candidates based on photometric criteria following the work of Cooke et al. (2014). A majority of confirmed LCEs in the literature to date have been selected for observations of LyC either based on already known spectral properties (e.g. spectroscopic redshift or O32 Vanzella et al. 2015; Izotov et al. 2016, 2018b) or involve targeting lensed galaxies (e.g. Bian et al. 2017; Vanzella et al. 2017) or narrow-band selected Ly α emitters (LAEs, Fletcher et al. 2018). Our approach, based on a purely photometric selection of candidate LCEs, represents a more efficient method of identifying a large sample of LCEs as we are not required to already have spectroscopic observations in hand or to focus on limited samples of lensed objects. The main driver of our method is to measure the total population of LCEs and study the full range of galaxy properties. We note, however, that this method also requires an accurate estimate of the photometric redshift, which currently limits us to well-surveyed fields with dense, multi-filter photometry.

This paper is organized as follows: in Section 2, we describe our photometric selection methodology and present our pilot sample of LCE candidates, in Section 3, we describe the observations and data reduction for our selected sample, in Section 4, we describe our analysis including both spectral measurement and photoionization modelling of optical line ratios, in Section 5, we present the results of these analyses, in Section 6, we discuss the implication of our results and evaluate the success of our selection methodology, and finally, in Section 7, we summarize our study and list our conclusions.

2 SAMPLE SELECTION

In this section, we describe the selection methodology of this pilot survey. The goal of our photometric selection approach is to identify star-forming galaxies at $z \gtrsim 3$ that are likely to be leaking LyC

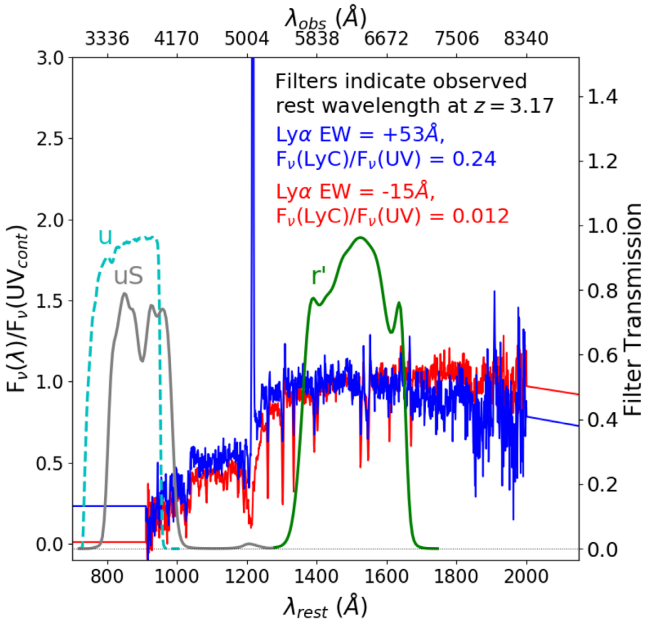

Figure 1. Composite Lyman break galaxy (LBG) spectra from Shapley et al. (2003) demonstrating to contribution from LyC photons in the *u* band. In blue and red, we show the stacked spectra for the highest and lowest quartiles in Ly α EW from LBGs in Shapley et al. (2003), respectively. Raw transmission curves for CFHTLS *uS* and r' filters are shown with wavelength coverage indicating the observed restframe wavelengths for galaxies at a redshift of $z = 3.17$ (observed wavelengths are shown on the top *x*-axis). At $z = 3.17$, the r' band probes the restframe UV continuum around 1500 Å, a wavelength regime commonly used in LyC escape studies (e.g. Steidel et al. 2018). We also show the CLAUDS *u* band, used to estimate f_{esc}(LyC) in Section 4.4, which has many advantages over the *uS* band as regards studying $z \sim 3$ LCEs (see Section 2.1.1).

photons into the IGM. This selection uses 30-band photometry from the Cosmic Evolution Survey (COSMOS, Scoville et al. 2007) field, including FourStar galaxy evolution survey (ZFOURGE Straatman et al. 2016) deep medium-band imaging. The depth and wavelength coverage of this photometric dataset provides photometric redshifts with accuracies of $\Delta z < 2$ per cent due to deep medium-band filter observations probing the Balmer break. Using galaxies from the ZFOURGE survey enables us to reliably select galaxies at $z > 3.0$.

LyC emitting galaxies at $z > 3.0$ will have some contribution from LyC photons in the *u* band, making this the critical observation band for our selection. This is demonstrated in Fig. 1 where we show stacked Lyman break galaxy (LBG) spectra from Shapley et al. (2003) where the top and bottom quartiles in Ly α equivalent width (EW) are shown in blue and red, respectively. The lower *x*-axis indicates restframe wavelengths while the upper x-axis shows the observed wavelengths at the average redshift of our final sample, $\langle z \rangle = 3.17$. We have overplotted the Canada France Hawaii Telescope (CFHT) *uS* and r' band transmission curves for comparison, indicating the spectral regions probed by these bands for LBGs at $z = 3.17$. We have also plotted the transmission curve of the CFHT Large-Area U-band Deep Survey (CLAUDS, Sawicki et al. in preparation) *u* band with a cyan dashed line. This filter is essential for estimating the level of LyC escape in our galaxy sample as described in Section 4.4; however, we note that this filter was not available when our sample was selected. At this redshift, observed flux in the *uS* band is made up of contributions from both LyC and Ly α forest photons.

In Fig. 1, we have also added LyC flux to the LBG spectra below $\lambda_{rest} = 912$ Å, constant in $F_\nu(\lambda)$, representing escaping LyC flux. The level of the added flux is chosen as a fraction of the UV continuum flux, $F_\nu(UV)$, defined as the median flux in the wavelength range 1450 Å $< \lambda <$ 1550 Å. The two values of F_ν(LyC)/$F_\nu(UV)$ of 0.24 and 0.012 shown in Fig. 1 correspond to $f_{esc,\,rel}$(LyC) = 1.0 and $f_{esc,\,rel}$(LyC) = 0.05, respectively, assuming an intrinsic LyC to UV flux ratio of 0.33 (e.g. Vanzella et al. 2012) and an IGM attenuation at 912 Å of 0.72. This latter assumption is taken as the average value of the $z = 3.17$ IGM attenuation at 912 Å computed following the models presented by Inoue et al. (2014). We must clarify that here $f_{esc,\,rel}$ is the relative escape fraction, and a dust correction must be applied to the observed $F_\nu(UV)$ to assess the absolute escape fraction (see Section 4.4 for complete definitions of $f_{esc,\,rel}$(LyC) and f_{esc}(LyC)).

Galaxies selected using the criteria described here are part of a pilot program to obtain optical emission lines using the Multi-Object Spectrometer for Infra-Red Exploration (MOSFIRE) instrument (this paper) and to detect LyC emission using the Low-Resolution Imaging Spectrometer (LRIS, Oke, Postman & Lubin 1998; Steidel et al. 2004) instrument (Meštrić et al. in preparation).

2.1 Photometric galaxy selection

The goal of our sample selection for the galaxies presented in this paper was to identify galaxies near $z \sim 3$ that are likely to exhibit non-zero LyC escape fractions, and to select those with LyC fluxes that could be detected during a single night of LRIS observations. As described in Section 4.4, an increase in LyC flux for galaxies at $z \sim 3.17$ will produce an increase in the observed *uS* band flux beyond what is expected from Ly α forest photons alone. Thus, for our sample, we select from those galaxies at $z \simeq 3$ with the brightest *uS* fluxes from our parent sample.

Although selecting galaxies at $z > 3.7$, where the *uS* band will have little or no contribution from $\lambda > 912$ Å photons, will produce a cleaner selection of LyC emitters, we select galaxies close to $z = 3.0$ for three reasons:

(i) Galaxies must be at $z \gtrsim 2.5$ for LyC photons to be detectable by ground-based spectroscopy (e.g. LRIS); however, the intrinsic faintness of LCEs along with the sensitivity of UV detectors at very short wavelength puts an effective lower redshift limit of $z \simeq 2.9$ for ground-based observations

(ii) From $z = 4.0$ to $z = 3.0$, the average transmission of the IGM to radiation at 912 Å increases from ∼0.4 to ∼0.7 (Inoue et al. 2014)

(iii) Observing galaxies at $z = 3.0$ provides a gain in brightness of ∼0.5 mag compared to $z = 4.0$

Given these three factors, for galaxies with the same $L(LyC)$ and f_{esc}(LyC), we expect those at $z \sim 3$ to be the most likely to have LyC spectroscopically detected in a single night of observations.

This selection requires a parent sample of galaxies with accurate photometric redshifts above $z \simeq 3$ to be sure that the *uS* band samples significantly the LyC portion of the spectrum. For this reason, our sample is pre-selected from the ZFOURGE survey (Straatman et al. 2016). Using SED fitting to up to 30 photometric bands, ZFOURGE provides medium-band, IR, photometric redshift accuracy of Δz <2 per cent up to $z = 4.0$ (with a maximum value at $z = 3.0 - 4.0$ of $\Delta z \simeq 5$ per cent). Furthermore, the ZFOURGE survey footprints are in HST legacy fields, thus providing space-based imaging to check for line of sight contaminants (e.g. Vanzella et al. 2010, 2012). Initial ZFOURGE SED fits include the *uS* band using templates assuming

f_{esc}(LyC) = 0.0 (i.e. LBG-like spectra); however, we performed additional SED fits for our candidate galaxies excluding the *uS* band with no significant change in photometric redshift. We also note that ZFOURGE galaxies are selected based on *Ks* band magnitude, thus low-mass galaxies may be missing from their catalogs (Spitler et al. 2014).

After our ZFOURGE photometric redshift pre-selection, our main selection criterion is that galaxies are sufficiently bright in the *uS* band such that their rest-frame UV spectra can be observed in a single night of LRIS observations. We estimate, based on previous experience, that our *uS* detection limit for our instrumental setup is 26-26.5 mag with the evidence of fainter continuum flux using spectral binning. In the context of LyC emitting galaxies, those galaxies with the highest *uS* flux at $z \simeq 3$ are the most likely to have nonzero f_{esc}(LyC), assuming galaxies are selected at a similar *Ks* band luminosity (i.e. similar stellar mass). Nonzero f_{esc}(LyC) would manifest as an excess *uS* flux relative to what is expected assuming the observed *uS* flux originates entirely from Ly α forest photons (see also Section 4.4).

Following the criteria described above, we focus our selection on galaxies with ZFOURGE photometric redshifts of $z \simeq 3.2$ with brighter than expected *uS* magnitudes. We are also limited on the sky by the fact that our observations comprised of a single MOSFIRE mask resulting in a final sample of eight galaxies. The fact that our observations were limited to a single MOSFIRE mask also means that only 3/8 galaxies are brighter than 26.5 mag in *uS*. The remaining galaxies were selected as the brightest *uS*-detected galaxies falling within the footprint of our MOSFIRE mask. Any additional unfilled slit positions were used for ZFOURGE targets from other observational programs.

The basic properties of our eight galaxies observed with MOSFIRE are described in Table 1 and CFHT Legacy Survey (CFHTLS) *uS* images are shown in the middle row of Fig. 2. Table 1 shows that 6/8 selected galaxies are well detected in the *uS* band, having *uS* magnitude errors smaller than m = 0.25. As stated, this is deliberate as brighter uS targets are the most likely to be detected at LyC in a single LRIS night (or ∼6 h exposure). Also included in Table 1 are the r' band magnitudes, which correspond roughly to the restframe 1500 Å continuum at the redshifts of our sample, for comparison to other works. Finally, it should be noted that galaxies in our selected sample fall within the standard LBG ($g - r$) vs ($u - g$) selection box (e.g. Steidel et al. 1996) and would thus be classified as LBGs.

Considering a parent sample of 717 galaxies from the ZFOURGE COSMOS field in the redshift range $2.9 < z < 3.2$, the three brightest targets in our sample are among the brightest 25 per cent in *uS*. The remainder of our sample range from being among the brightest 31 per cent to 59 per cent. Our ongoing sample selection of LyC detected galaxies requires careful visual inspection of images, and, on average, we exclude ∼95–98 per cent of galaxies in our target redshift range. Typically, galaxies with $uS > 26.5$ mag are contaminated by nearby sources (either stars or bright, low-redshift galaxies) while sources fainter than 26.5 are very often found to be either multiple sources in HST imaging (possible low-redshift interlopers or mergers) or undetected in *uS*. The majority of our current selections of LyC-detected galaxies fall in the range between $27.5 < uS < 26.5$, similar to the sample presented here. The one caveat here is that, as we describe in Section 6.2, ongoing sample selection has shifted to $z > 3.4$ as a result of now using the CLAUDS *u* band filter (described below). A more detailed description of our ongoing selection of photometrically detected LyC-emitting galaxies will be presented in Cooke et al. (in preparation) and Meštrić et al. (in preparation).

We also estimate f_{esc}(LyC) for our sample from *u* band photometry using Shapley et al. (2003) LBG spectral stacks (as shown in Fig. 1) as templates for the underlying spectra of our sample in Section 4.4. This estimate is made using CFHT Large-Area U-band Deep Survey (CLAUDS, Sawicki et al. in preparation) imaging, shown in the bottom row of Fig. 2, rather than CFHTLS *uS* for three reasons: CLAUDS imaging is deeper having a depth of ∼27–28 mag (depending on position on the field), the new *u* filter used in CLAUDS does not suffer from red-leak issues as described in Section 2.1.1, and it covers bluer wavelengths having less contribution from the Lyα forest (see Fig. 1). We note that CLAUDS imaging was not available during the initial selection of our sample, and thus was not included in our selection criteria.

Finally, we comment on the possibility of whether any of the eight galaxies in our sample harbour active galactic nuclei (AGN). This issue has been explored by the ZFOURGE team in Cowley et al. (2016) where galaxies are examined in X-ray, radio, and infrared (IR) data for evidence of AGN activity. All eight galaxies in our sample are not identified as AGN using any these data sets. It should be noted though, that the redshift of our sample is near the upper limit for AGN identification by these methods. Cowley et al. (2016) estimate a lower limit for detecting radio AGN of $L_{1.4\,GHz} = 1.9 \times 10^{24}$ W Hz^{-1} and for X-ray AGN of $L_X = 7.0 \times 10^{42}$ ergs s^{-1} at $1.8 < z < 3.2$. Galaxies in our sample are also only weakly detected in the IR 4.5, 8.0, and 24 μm bands (or not detected in the case of 13459) thus, from ZFOURGE data, it was not possible to rule out the possibility of weak AGN activity in our sample at the time of sample selection. After our spectroscopic observations, however, our deep LRIS spectra strongly rule out AGN, which are easily identified in the FUV through detection of high ionization emission lines such as N V (λλ1240 Å), O VI (λλ1035 Å), or C III (λλ1907 Å, Shull, Stevans & Danforth 2012). These are completely absent from our observations.

2.1.1 *Sample selection caveats*

The first caveat regarding selecting only those galaxies with strong *uS* band detections is the danger of line-of-sight contamination from low-*z* galaxies. This occurs where less luminous galaxies at $z < 3$ fall at a low angular separation from a target galaxy such that the two galaxies are not well resolved in ground-based photometry. Indeed, low-redshift interlopers have been found to refute suspected LyC detections in recent studies at high redshift (Vanzella et al. 2010, 2012). Quantitatively, Cooke et al. (2014) use CFHTLS to estimate that, for $z = 3$–4 galaxies down to a *u* magnitude of ∼28,one can expect a ∼5–7 per cent rate of line-of-sight contamination from lower redshift galaxies in standard 2.″0 apertures and SExtractor-based detections (consistent with previous searches for LCEs, e.g. Shapley et al. 2006; Nestor et al. 2011).

The ZFOURGE survey includes Hubble Space Telescope (HST) photometry in 3–4 bands (depending on the location of a given galaxy), allowing us to check for low-*z* companions at 0.05 arcsec/pixel spatial resolution. We show RBG colour-composite images for our sample in the top row of Fig. 2. Here, the R, G, and B images come from the HST F160W, F125W, and F814W, respectively. HST images of our sample show a range of morphologies, including single clumps, elongation, and multiple continuum peaks. The origin of the apparent clumpy nature of these galaxies is unclear due to the fact that we are sampling the restframe UV and blue optical portion of the spectrum for star-forming galaxies (Elmegreen et al. 2005; Förster Schreiber et al. 2011; Swinbank

Table 1. Basic properties of photometrically selected MOSFIRE target galaxies.

ID	RA deg.	DEC deg.	z^a	$\log_{10}(\mathcal{M}_*)^b$ ($M_\odot$)	$\log_{10}(SFR)^c$ ($M_\odot yr^{-1}$)	*uS* (mag)	r' (mag)	*Ks* (mag)
12676	150.21806	2.31344	3.12	9.80	1.92	26.53 ± 0.22	24.71 ± 0.04	23.47 ± 0.08
13459	150.20192	2.32179	3.18	9.75	0.75[d]	26.63 ± 0.30	24.72 ± 0.03	23.59 ± 0.08
14528	150.15553	2.33388	3.08	9.49	1.70	26.61 ± 0.21	24.75 ± 0.04	23.92 ± 0.09
15332	150.16920	2.34218	3.21	9.68	1.70	26.78 ± 0.23	24.95 ± 0.06	24.10 ± 0.10
15625	150.13919	2.34531	3.23	9.77	1.58	27.29 ± 0.36	24.82 ± 0.04	23.50 ± 0.07
16067	150.20010	2.34941	3.21	9.19	1.81	26.06 ± 0.13	24.02 ± 0.02	22.90 ± 0.04
17251	150.13780	2.36102	3.12	10.06	2.09	25.68 ± 0.12	23.15 ± 0.03	22.86 ± 0.05
17800	150.17387	2.36797	3.21	9.43	1.90	26.28 ± 0.19	24.26 ± 0.03	23.46 ± 0.07

Notes. [a]ZFOURGE photometric redshift
[b]Stellar Mass measured from ZFOURGE SED fitting with emission lines included
[c]ZFOURGE UV + IR SFR (Chabrier 2003, IMF), with IR data coming from Spitzer/MIPS and Herschel/PACS observations (Tomczak et al. 2016)
[d]SFR for galaxy 13459 is based on UV alone as it is undetected in the far IR bands

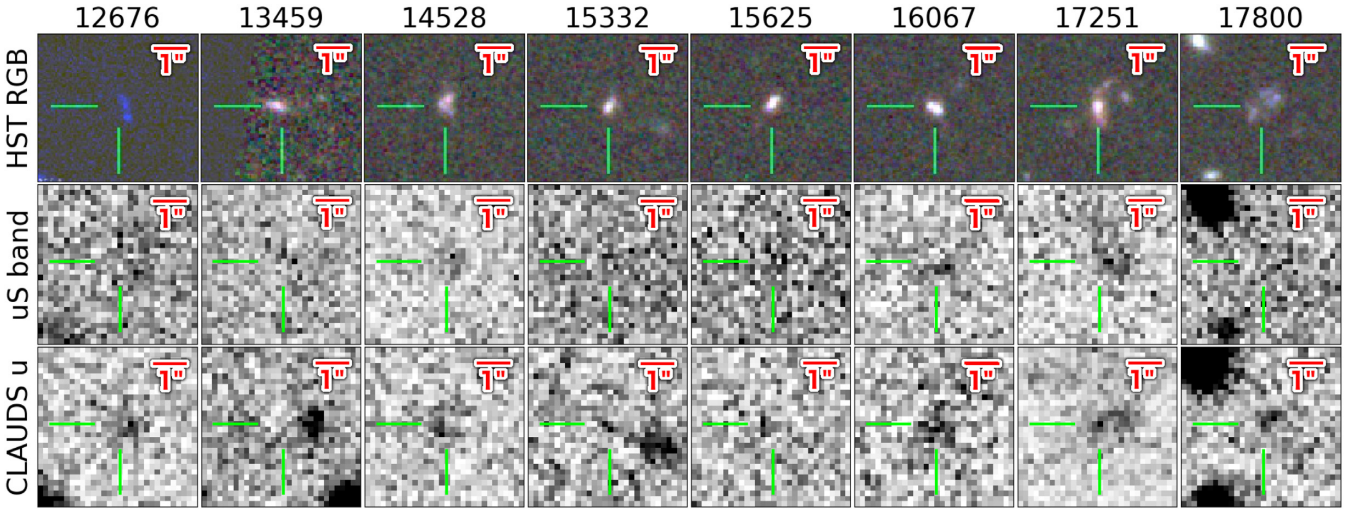

Figure 2. *Top:* RGB images for our selected galaxies produced using HST F160W, F125W and F814W filters (galaxy 12676 only has coverage in F814W). HST imaging shows galaxies in our sample to be elongated, nonsymmetric, and/or exhibiting multiple continuum peaks. These features may be indicative of ongoing mergers; however, we cannot fully rule out the possibility of low-redshift, line-of-sight companions. Although there is no evidence from our MOSFIRE spectra of such companions, this possibility will affect our selection, and we discuss the implications of this in Section 6.2 *Middle:* CFHTLS *uS* images of our galaxy sample. *Bottom:* CLAUDS *u* band images of our galaxy sample that are used in estimating f_{esc}(LyC) in Section 4.4.

et al. 2011; Wisnioski et al. 2012). It is possible these are signatures of multiple, large star-forming regions or ongoing mergers. We have not excluded possible mergers from this pilot survey based on HST morphology as we are also interested in the role that galaxy mergers play in LyC escape. The effect of mergers on optical diagnostics is discussed further in Sections 5.1.1 and 6.3.

The second caveat to our selection is that there is a known issue of redleak in the CFHT *uS* filter, which overlaps with Ly α at $z \sim 3.17$ (see Fig. 1). This means that the observed *uS* band flux contains ~1 per cent of the flux from redder UV continuum and/or Ly α. We simulate this effect for each of the five galaxies in our sample that are known LAEs from our LRIS spectroscopy with Ly α EW in the range from 20 to 104 Å (see Table 3). This is done by replacing the Ly α emission line in stacked LBG spectra from Shapley et al. (2003) with a Gaussian profile having an EW matching the observed value. Here, we use the stacked LBG spectrum from Shapley et al. (2003) representing the top quartile in Ly α EW. We then shift the observed wavelengths of the spectrum to match the redshift of a given galaxy and measure the relative contribution to the *uS* band flux from photons in the redleak portion of the transmission curve. At a given redshift, the redleak contribution to *uS* mag will depend on both f_{esc}(LyC) and Lyα EW, with the maximum occurring at low f_{esc}(LyC) and high Lyα EW. In the case of $f_{esc}(LyC) = 0.0$, we estimate a maximum redleak contribution to the *uS* flux of 8–17 per cent for LAEs in our sample. Thus, even in the worst case, redleak will have minimal impact on our sample selection. All future samples for this program eliminate this issue by using deep CLAUDS *u*-band data, which does not suffer from redleak.

The final caveat to our pilot survey sample selection is the fact that, as we have mentioned, at $z < 3.6$ the observed *uS* magnitudes will also be influenced by photons from the Lyα forest ($\lambda > 912$ Å). Clearly, this limits our ability to select high f_{esc}(LyC) galaxies based on *uS* magnitude alone at $z \sim 3.2$. As we have noted, we select galaxies bright in the *uS* band for this pilot study to ensure spectral detection of UV photons with LRIS in a single night of observations, thus biasing our sample towards lower redshifts. We note that the CLAUDS *u* band, which we use to estimate f_{esc}(LyC) in Section 4.4 has a sharp cutoff at ~4000 Å thus reducing this issue.

The results of this pilot study inform more stringent photometric selection criteria aimed at selecting exclusively high f_{esc}(LyC) targets for future observations. Most importantly, targets are selected at $z > 3.4$ to ensure that detected u band flux originates in the LyC portion of the galaxy SED. This is described further in Section 6.2 and Cooke et al. (in preparation).

3 OBSERVATIONS AND DATA REDUCTION

3.1 MOSFIRE

MOSFIRE observations for this study were performed on 01 February 2015. Of particular interest for our study is the line ratio of [O III] (λ5007 Å) to [O II] (λλ3727 Å). Targeting these lines (with the addition of H β) requires us to observe in both the H-band and K-band (targeting [O II] and [O III] at $z \sim 3.17$, respectively).

For each band, we estimate the average seeing using the continuum detection of the flux calibration star observed in a slit with a width of 3.0 arcsec. We first identify windows in the 2D stellar spectrum that have both a relatively strong continuum detection and lack large residuals from sky line subtraction. We construct multiple profiles of our continuum detection along the slit by averaging along the spectral direction in each of these windows. We then fit these profiles using a Gaussian function. We take the final seeing (given below for each band) as the average value of all full width half max (FWHM) of our Gaussian fits for each clear spectral window for a given band.

K-band observations were performed using the standard MOSFIRE slit width of 0.7 arcsec with a resolution of $R = 3610$ (velocity resolution $\sim$40 km s^{-1}) and an average seeing of 0.79 arcsec. The total, on-source integration time was 3 h using an ABAB dither sequence with the offset position separated by 3.0 arcsec along the slit. Individual exposures were 180 s with the full integration composed of three sets of 20 exposures. For the eight galaxies in our MOSFIRE sample, we find a signal to noise of our [O III] (λ5007 Å) line flux ranging from 5.2 to 42.1 with an average value of 23.0. Here, our noise is defined as the integral of a Gaussian function with a central flux density equal to the one sigma spread of our noise spectrum at the location of a given line and a line width equal to that measured for the line (line fitting is described in detail in Section 4.1).

H-band observations were performed similarly, using the same 0.7 arcsec slit with a slightly higher resolution of $R = 3660$ and an average seeing of 0.96 arcsec. Given that the H-band is slightly less sensitive than the K band, the total on-source integration time was increased to 3 h and 20 min. This was achieved using the same ABAB dither pattern using two sets of 30 exposures and two sets of 20 exposures with individual times of 120 s. Among the 7/8 galaxies detected in [O II] (λλ3727 Å), this strategy provides a signal to noise ranging from 4.3 to 19.9 with an average value of 10.6.

The data reduction was performed in two steps. A detailed description of this reduction can be found in Nanayakkara et al. (2016), and we describe it only briefly here.

First, a custom version of the public MOSFIRE data reduction pipeline from the 2015A semester was used to reduce the raw data into individual 2D spectra for each object. This step includes flat-fielding, thermal background subtraction (K band), wavelength calibration, a barycentric correction to the wavelength solution, careful sky-subtraction following Kelson (2003), and rectification. The calibration provides spectra with vacuum wavelengths with a residual error of <0.1 Å.

Next, a flux calibration was performed using a custom IDL package. For our study, an accurate flux calibration is essential for measuring the emission line ratio of [O III] to [O II] given they fall in separate bands. A standard star HIP 43018 of A0V type was observed in the MOSFIRE long-slit 'long2pos' mask with a slit width of 0.7 arcsec. We used the standard star for both the telluric correction and flux calibration. Note that the seeing during the standard star observation was $\sim$0.8 arcsec in both the H and the K band, yielding a constant absolute flux calibration offset due to slit-loss. Slit-loss from the standard star does not affect the line ratio measurements between the H and K bands because the flux offset in each band is constant. Hydrogen absorption lines are removed from the standard star spectra using Gaussian fits and the resulting spectra are divided by a blackbody function with the temperature given by the expected temperature of the standard star. The resulting spectra are normalized, smoothed, and are assumed as the sensitivity curves of our H- and K-band observations. We apply these curves to the standard star observations, then compare the flux density in the given band to the expected values from the 2MASS catalogue (Skrutskie et al. 2006), thus calculating the factor used to convert data-units to flux-units.

Finally, the difference in seeing between our K and H band observations (0.79 arcsec versus 0.96 arcsec) may result in a larger portion of the emission line flux being blurred outside of our 0.7 arcec slit for our H-band observations (i.e. larger slit loss for galaxy observations). This results in a relative underestimation of the [O II] (λλ3727 Å) flux when compared to [O III] (λ5007 Å), and thus an overestimation of the [O III] (λ5007 Å)/[O II] (λλ3727 Å) ratio. We make a quantitative estimate of this effect for each galaxy by degrading the PSF of the HST F814W images to the K- and H-band values of 0.79 arcsec and 0.96 arcsec. We then compare the fraction of the flux falling within a pseudoslit matching our MOSFIRE slitmask. We find that, in order to compensate for the different fractions of the source falling inside the slit, the flux from the 0.96 arcsec image (corresponding to H-band observations) must be scaled by a factor of 1.12–1.25 depending on galaxy morphology and slit position. The slit loss correction values are quoted in Table 2. We apply this correction to the measured [O II] (λλ3727 Å) line fluxes prior to our correction for dust attenuation.

3.2 LRIS

LRIS observations for our MOSFIRE sample come from a larger sample of 22 galaxies selected in a similar method as that described in Section 2.1. These galaxies were observed on 19 March, 2015. The goal of our companion LRIS pilot program is the detection of LyC emission from star-forming galaxies at $z = 3.0$ and higher.

For our observations the instrumental setup was as follows. Our LRIS slit mask employed 1.2 arcsec slits and we use the 560 dichroic filter. Spectra were dispersed using the 400/3400 and 400/8500 gratings for the blue and red arm of LRIS, respectively. Each mask was observed with a series of 16 exposures. For the blue arm, exposure times were 1200 s giving a total time of 5.33 h and for the red arm exposure times were 1131 s giving a total time of 5.03 h. The average seeing for the sample presented here had a FWHM of $\sim$1.0 arcsec.

The LRIS data reduction was performed using the standard IRAF software procedures, the basic steps are as follows. First, a conversion is performed using the multi2simple task in the KECK.LRIS IRAF package, and during this process the overscan region is removed and bias corrections are performed. Master science frames

Table 2. MOSFIRE sample: optical line fluxes.

ID	[O II] ($\lambda\lambda$3727)[a, b, c, d]	slit corr.	Hβ[a, b, c]	[O III] (4959) [a, b, c]	[O III] (5007) [a, b, c]	$z^{e}_{\rm spec}$	β^{f}	$E(B-V)$
12676	2.22 ± 0.18 (0.98)	1.25	–	1.45 ± 0.11 (0.94)	4.97 ± 0.36 (3.24)	3.07	−1.37	0.11
13459	$\leq$0.67 (0.41)	1.20	1.34 ± 0.11 (0.93)	1.36 ± 0.22 (0.96)	5.70 ± 0.18 (4.01)	3.09	−1.65	0.09
14528	11.47 ± 1.39 (5.71)	1.24	–	2.92 ± 0.09 (2.05)	10.03 ± 0.14 (7.07)	3.00	−1.64	0.09
15332	5.5 ± 2.1 (3.03)	1.12	1.19 ± 0.1 (0.83)	2.08 ± 0.11 (1.46)	5.83 ± 0.2 (4.1)	3.11	−1.55	0.09
15625	4.78 ± 0.87 (2.67)	1.23	1.62 ± 0.25 (1.22)	2.98 ± 0.12 (2.27)	8.82 ± 0.15 (6.72)	3.18	−1.81	0.07
16067	3.71 ± 0.37 (2.39)[g]	1.19	3.95 ± 0.15 (3.23)	7.89 ± 0.16 (6.48)	23.37 ± 0.21 (19.24)	3.19	−2.09	0.05
17251	14.6 ± 3.01 (6.5)	1.18	0.42 ± 0.09 (0.26)	0.85 ± 0.16 (0.53)	2.82 ± 0.23 (1.77)	2.99	−1.31	0.12
17800	2.32 ± 0.5 (1.53)	1.16	1.58 ± 0.25 (1.29)	1.79 ± 0.14 (1.47)	6.49 ± 0.2 (5.34)	3.17	−2.09	0.05

Notes. [a]Emission line fluxes are in units of 10^{-17} ergs s^{-1} cm^{-2}.
[b]Corrected for internal extinction based on $E(B-V)$ calculated from the UV slope β.
assuming a SMC attenuation curve and $E(B-V)_{\rm stars} = E(B-V)_{\rm gas}$.
[c]Non-dust corrected fluxes given in parentheses.
[d][O II] ($\lambda\lambda$3727) multiplied by value in next column to account for slit loss as described in Section 3.1.
[e]Spectroscopic redshift from fit to K-band data. We estimate an uncertainty of $\Delta z = 0.0011$, the average difference between the K- and H-band spectroscopic redshifts for our sample.
[f]UV continuum slope measured at $\lambda_{\rm rest} \simeq$ 1250–3000 Å.
[g][O II] ($\lambda\lambda$3727 Å) possibly overestimated due to OH contamination, see Section 4.1.

for each target are produced by averaging all single exposures using imcombine and each master frame is flat-fielded using a master flat produced from our twilight spectra. Next, apall is used to extract the 1D from the 2D spectra, and background subtraction is also performed during this step. We then apply a wavelength solution extracted from arc lamp observations. Finally, we apply a flux calibration based on standard star observations performed on the same night as our science observations.

Analysis of the full LRIS data set is ongoing. More details on our data reduction process and a full spectral analysis of LyC emission in our full sample will be the subject of future work (Meštrić et al. in preparation). In this work, Ly α properties of our LRIS spectra are used to produce matched template spectra for estimating $f_{\rm esc}$(LyC) from photometric observations in Section 4.4. A careful assessment of LyC emission in stacked LRIS spectra will be included in Meštrić et al. (in preparation).

4 ANALYSIS

4.1 Optical emission line fitting

For the MOSFIRE H and K bands, we simultaneously fit all emission lines in that band using Gaussian profiles. The free parameters in each fit are the peak flux densities at the centres of each line (A_λ), the continuum level, a fixed line width, and the redshift, where the latter two values are assumed to be the same for all lines. Although none of our galaxies have continuum detected in our spectra, the continuum level in our fit accounts for any residual zero-point offsets from our data reduction. Our fits are thus performed with five and six free parameters for H- and K band, respectively. Finally, we note that galaxy 12676 exhibits a complex line shape for [O III] (λ5007 Å), possibly due to the multiple components seen in the HST imaging in Fig. 2. Thus, we include a second Gaussian component for this line allowing the line width and redshift to vary relative to the other components. This approach has only a minor effect on the measured line flux and negligible effect on our resulting emission line ratios. MOSFIRE emission line fits are illustrated in Fig. 3, where reduced 1D spectra are shown in red and our emission line fits are shown in blue. Line fluxes for each line are calculated from our Gaussian fits as:

$$F(\lambda) = \sqrt{2\pi} A_\lambda \sigma. \quad (1)$$

Fig. 3 illustrates that, in the H band, the [O II] doublet is not well resolved. In most cases, both Gaussian components are required to provide a reasonable fit to the data. In cases where the [O II] doublet is well fit by a single Gaussian profile, we take the flux of this single Gaussian as the total [O II] ($\lambda\lambda$3727 Å) flux. Thus, regardless of the relative flux of the two lines, our fitting procedure accounts for the total flux of the observed doublet.

We calculate the error of our emission line fluxes by combining the observed spectra with the error spectrum extracted during our data reduction. For each spectrum, we create 1000 realizations of possible noise spectra by selecting random values in each spectral bin from a Gaussian distribution with a σ equal to the error spectrum in that bin. We then combine each noise spectrum with the best-fit spectra to create 1000 artificial observations. We then refit the spectral lines in these artificial observations, and the error in flux for each line is taken as the standard deviation of computed values.

We also make a rough estimate of the upper limit of the [O II] ($\lambda\lambda$3727 Å) flux for galaxy 13459 allowing for limits to be placed on emission line ratios in Section 5.1. The upper limit here is simply taken as three times the Gaussian noise in the 1D H-band spectrum for this galaxy. We do not include similar limits on the H β flux for galaxies 12676 and 14528 as the former is contaminated by strong skyline residuals and the latter has H β falling below the spectral coverage of our observations.

From Fig. 3, galaxy 16067 appears to have a very large ratio of the [O II] doublet (λ3729 Å/λ3726 Å), which has been shown by Sanders et al. (2016) to have a maximum theoretical value of $\sim$1.45. For galaxy 16067, we obtain a value of 1.96, significantly higher than the theoretical limit. We randomly generate 10 000 simulated line ratios for this galaxy where each time both line fluxes are independently varied within a normal distribution having a σ defined by the computed error (as described above). Among the simulated line ratios, only $\sim$4 per cent fall below the theoretical upper limit, thus the computed doublet ratio for galaxy 16067 is unreasonably large, even within our measured uncertainties. The most likely cause is significant OH emission overlapping with the [O II] (λ3729 Å) line. We retain the measured, though implausible, value in our analysis with the caveat that the total [O II] flux is likely an overestimate. The ultimate result of this overestimate is that the O32 measurement for galaxy 16067 is likely underestimated, a caveat that we carry throughout this work. Overall, this would not

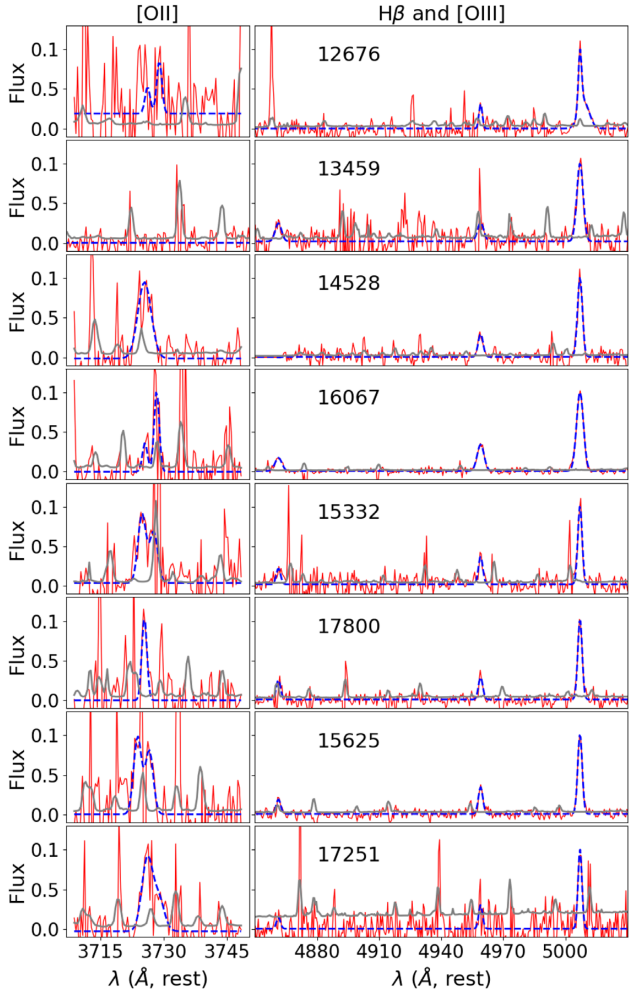

Figure 3. MOSFIRE spectra for *uS* selected $z \sim 3$ galaxies in our sample. Red lines show the observed spectra whereas blue dashed lines show our emission line fits as described in Section 4.1. The grey lines show the error spectrum. For all galaxies shown here, the [O II] doublet is observed in the H-band while H β and the [O III] doublet both fall in the K-band. H-band data are plotted normalized by the maximum flux in our [O II] line fits, and, similarly, K-band data are plotted normalized by the peak flux of our [O III] and H β line fit. Dust-corrected line fluxes are given in Table 2.

alter the conclusions of this work. We also note that the [O II] doublet ratios of the remaining galaxies where both lines are well resolved are well within the theoretical limits presented in Sanders et al. (2016).

4.2 Attenuation correction

Line fluxes for each galaxy are corrected for internal dust attenuation, which is estimated based on the observed slope of the ultraviolet (UV) continuum emission, β. Here, fits are of the form $F(\lambda) \propto \lambda^{\beta}$. This is a common technique in the literature based on the IRX-β relation of Meurer, Heckman & Calzetti (1999). For our sample, we measure the slope of the rest-frame UV light from the ZFOURGE photometry in the wavelength range from ∼5200–10500 Å corresponding to restframe wavelengths of ∼1250–2500 Å at the redshift of our sample. This restframe wavelength used for fitting to β range matches that recommended by Calzetti, Kinney & Storchi-Bergmann (1994). For COSMOS data, this includes

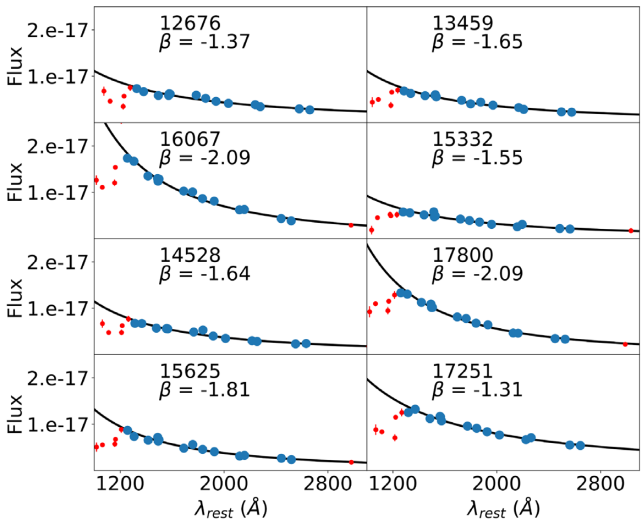

Figure 4. Exponential fits to the restframe photometric data (ZFOURGE) for galaxies in our sample. The y-axes indicate flux in units of ergs s^{-1} cm^{-2} $Å^{-1}$. Model fits, indicated by the solid black lines, are of the form $F(\lambda) \propto \lambda^{\beta}$. Data from photometric bands used in our fits are shown in blue while data below restframe ∼1200 Å (shown in red), below which the galaxy SED deviates significantly from an exponential behavior as a result of Ly α absorption. The final fitted values of β are indicated in each panel.

14 photometric bands for performing our fit to β. UV continuum fits for galaxies in our MOSFIRE sample are shown in Fig. 4.

Next, we must convert the observed β values to a reddening, $E(B-V)$, in order to apply a dust correction at longer wavelengths. Following Reddy et al. (2018), we assume the Small Magellanic Cloud (SMC) attenuation curve from Gordon & Clayton (1998) and an intrinsic UV continuum slope of $\beta_0 = -2.616$. This is a steeper UV continuum slope than is typical of low redshift star-forming galaxies; however, there is growing evidence that such a steep slope may be common at high-redshift. Reddy et al. (2018) show that together, these assumptions result in a relationship of:

$$E(B-V) = 0.232 + 0.089 \times \beta, \quad (2)$$

which we use to calculate $E(B-V)$ for each of our galaxies.

We also assume that the nebular and stellar attenuation are equivalent rather than applying the correction of $E(B-V)_* = 0.44 \times E(B-V)_{\rm gas}$ typically applied to low-redshift star-forming galaxies (Calzetti et al. 2000). Recent works have shown that attenuation in highly star-forming galaxies at both high- and low-redshift are better described by the relation $E(B-V)_* = E(B-V)_{\rm gas}$ (Erb et al. 2006; Reddy et al. 2010; Kashino et al. 2013; Reddy et al. 2015; Bassett et al. 2017a).

Finally, the resulting $E(B-V)$ is then applied, along with our chosen SMC attenuation curve, to the observed optical emission line fluxes. The final, dust-corrected emission line fluxes, as well as the measured β and $E(B-V)$ values, are shown in Table 2. Given the low levels of attenuation found for galaxies in our sample, assuming different dust curves (e.g. Calzetti et al. 2000; Cardelli, Clayton & Mathis 1989) or applying a factor of 0.44 to convert stellar $E(B-V)$ to a nebular value will have little effect on our final results.

4.3 Photoionization modelling

We calculate a variety of photoionization models using the publicly available Modeling And Prediction in PhotoIonized Nebulae

and Gasdynamical Shocks (MAPPINGS) V code (see Allen et al. 2008, for the most recent publication regarding a previous release). MAPPINGS V is a photoionization modelling code that performs 1D radiative transfer calculations in order to model the emission line fluxes of various astrophysical sources including H II regions, planetary nebulae, and active galactic nuclei. MAPPINGS V inputs include a source spectral energy distribution (SED), nebular abundances, physical parameters (e.g. density, pressure, ionization parameter, etc.), atomic line data from the laboratory, and dust depletion data (among others).

For this work we calculate two types of H II region models for comparison with our MOSFIRE sample. Specifically, these represent ionization-bounded and density-bounded H II regions. We describe these two classes of models in the remainder of this section. The relevant outputs taken from MAPPINGS V for our work are the optical emission lines [O II] (λλ3727 Å), [O III] (λ4959 Å), [O III] (λ5007 Å), and H β, which we compare with the values observed in our sample.

Ionization-bounded models represent H II regions in which all ionizing photons produced by the central source(s) (e.g. LyC photons) are absorbed and re-emitted at longer wavelengths as a variety of optical and IR emission lines. This type of model results in a shell-like structure, with highly ionized gas at the centre surrounded by a shell of neutral gas. Ionization-bounded models are very commonly assumed for H II regions in low-redshift star-forming galaxies and correspond to the conditions often referred to as Case-B recombination (Osterbrock 1989).

We calculate emission line fluxes for ionization-bounded nebulae using MAPPINGS V, with a fixed, isobaric gas pressure of $P/k = 10^5$ cm^{-3} K and a fixed gas temperature of 10^4 K. This can be converted to a constant H II density, n_H, as $n_H \propto P/T$. The proportionality factor varies slightly with metallicity resulting in densities of $n_H \simeq 3.9$ cm^{-3} at low metallicity and $n_H \simeq 6.5$ cm^{-3} at high metallicity (corresponding electron densities, n_e, are 4.0 cm^{-3} and 6.8 cm^{-3}). We assume a two-sided, plane-parallel geometry, and a gas filling factor of 1.0. Grids of models are calculated by varying the ionization parameter, $q_{\rm ion}$, defined as:

$$q_{\rm ion} = \frac{Q_{H^0}}{4\pi R_s^2 n_H} \quad (3)$$

where Q_{H^0} is the number of hydrogen ionizing photons produced per second, R_s is the Strömgen radius, and n_H is the density of hydrogen. In this work we vary $q_{\rm ion}$ from $\log_{10}(q_{\rm ion}) = 6.5$ to $\log_{10}(q_{\rm ion}) = 8.5$ and varying metallicity from $12 + \log_{10}({\rm O/H}) = 7.86$ to $12 + \log_{10}({\rm O/H}) = 8.99$. The source of ionizing photons in all models is an SED of an instantaneous star-burst computed using STARBURST99 (Leitherer et al. 1999) and assuming a Salpeter (1955) initial mass function (IMF) with masses of individual stars in the range 0.1-100 $M_\odot$. We compute models at metallicities of $0.001 < Z < 0.04$, where stellar and nebular metallicities are matched similar to Nicholls et al. (2017), and SEDs are sampled at a starburst age of 1 Myr.

Density-bounded nebulae, on the other hand, are models in which the flux of ionizing photons from the central source is so large that the gas between the source and the observer is fully ionized. In these types of models, ionizing radiation is able to escape because there is little or no neutral gas remaining between the source and observer to absorb these photons. Thus, density bounded nebulae models are likely more relevant to discussion of galaxies with nonzero $f_{\rm esc}$(LyC). In MAPPINGS V, we produce density bounded models by specifying an optical depth limit for hydrogen (H I only), $\tau_{\rm H\,I}$. In practice this is achieved by varying the radius at which the output is evaluated at a fixed HI density. $\tau_{\rm H\,I}$ is converted to an $f_{\rm esc}$(LyC) as:

$$f_{\rm esc}({\rm LyC}) = e^{-\tau_{\rm H\,I}} \quad (4)$$

Similar to our ionization bounded models we calculate emission line fluxes for density bounded models at fixed gas pressure and temperature. We again vary the ionization parameter from $log_{10}(q_{ion}) = 6.5$–8.5 with each grid calculated at a fixed metallicity, varying $\tau_{\rm H\,I}$ from 200 to 0.001. This effectively corresponds to a variation in $f_{\rm esc}$(LyC) from ∼0.0 to 0.999 noting that for $f_{\rm esc}({\rm LyC}) = 1.0$, no emission lines would be present due to an absence of an ionized nebular region. We calculate three grids at fixed $12 + log_{10}(O/H) = 7.86$, 8.48, and 8.99.

Results of our photoionization modelling calculations are presented in Sections 5.2 and 6.3.

4.4 Estimating $f_{\rm esc}$(LyC) from photometry

In this Section we describe our method of estimating $f_{\rm esc}$(LyC) from our photometric measurements. Our process relies on a comparison of CLAUDS *u* band and *r* band fluxes that are extracted using identical apertures. The contribution to the observed *u* band flux from λ > 912 Å photons is modelled using linear combinations of stacked LBG spectra from Shapley et al. (2003). This process, which is necessitated by the fact that Ly α forest light also contributes to the observe *u* band flux at the redshift of our sample, is illustrated in Fig. 5.

The first step of this process is to construct a composite spectrum from stacked LBG spectra of Shapley et al. (2003) that best matches the Lyα emission in our observed LRIS spectrum, noting that 5/8 galaxies in our sample exhibit Ly α in emission. Comparing stacked LBG spectra with and without Ly α emission, LAEs are known to have a bluer UV continua (Cooke et al. 2014) and thus, similarly higher Ly α forest flux relative to the UV continuum normalized at 1500 Å when compared to LBGs with Ly α in absorption. These properties vary systematically with Ly α EW. Thus, a mismatch between our observed LRIS spectra and the Lyα properties in composite spectra can affect our estimates of $f_{\rm esc}$(LyC) from photometric observations. For our analysis we use a total of four composite spectra: one Ly α absorber and three composite spectra with increasing Ly α EW where composite spectra are constructed as linear combinations of stacked LBG spectra from Shapley et al. (2003) that best match the Lyα EW observed in our LRIS spectra. We test for the level of variation in $f_{\rm esc}$(LyC) that may be attributed to such a mismatch by estimating $f_{\rm esc}$(LyC) using all four composite spectra. For most galaxies, we find a variation of $\Delta f_{\rm esc}({\rm LyC}) < 0.05$ among all four composite spectra. Our lowest redshift galaxy, galaxy 17251, has a larger variation of 0.09 due to a larger contribution to the *u* band from the Lyα forest.

Next, the composite spectrum for each galaxy is normalised based on the observed *r* band flux in F_ν. At the average redshift of our sample of $\langle z \rangle = 3.17$, the *r*-band samples the rest-frame UV continuum around 1500 Å, which is the wavelength typically considered for measuring LyC escape (e.g. Steidel et al. 2018). The normilization factor for our composite spectrum is taken as the observed *r* band F_ν, $F_\nu(UV)$, divided by the median $F_\nu(UV)$ of the matched composite spectrum for a given galaxy. The matched composite spectrum is then multiplied by the normalization factor. In Fig. 5, we show the observed $F_\nu(UV)$ with the black dashed line and the normalized composite spectrum with the solid blue line. The resulting spectral regions blueward of Ly α is assumed to match the underlying spectra of our galaxy sample. This appears reasonable as we find a good agreement between normalized composite spectra and the

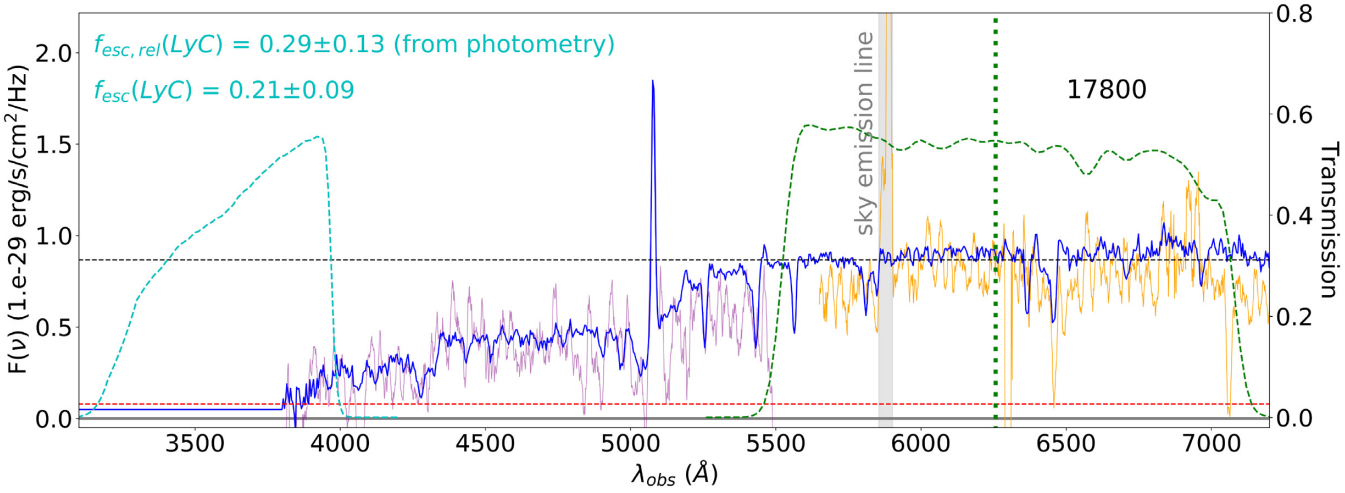

Figure 5. An illustration of our method of estimating f_{esc}(LyC) from CLAUDS *u* band photometry for galaxy 17800. CLAUDS *u* and *r* transmission curves (with atmospheric transmission, optics throughput, and CCD quantum efficiency accounted for) are shown by cyan and green dashed lines, respectively, with transmission given by the right *y*-axis. Corresponding observed F_ν in the *u* and *r* bands are shown by the horizontal red and black dashed lines, respectively. The composite spectrum, constructed from stacked LBG spectra of Shapley et al. (2003), is normalized based on the *r* band flux and is shown by the solid blue line. Our LRIS spectrum, which has been smoothed using a tophat filter with a width of 20 Å, for the blue and red arms are shown in purple and orange, respectively (note that the quoted f_{esc}(LyC) is *not* measured from the LRIS spectrum). The estimated value for photometric f_{esc}(LyC) is annotated in the upper left. Finally, we indicate $\lambda_{rest} = 1500$ Å with a green, vertical dotted line.

observed *u* and *g* magnitudes. For comparison, we also show an observed LRIS spectrum, which has been smoothed using a tophat function with a width of 20 Å, and it can be seen that the composite spectrum is indeed well-matched to the observed spectrum at blueward of Ly α. Finally, we note that at observed wavelengths below restframe 912 Å, composite spectra have a flux density of 0.

Having produced a normalized composite spectrum for each galaxy, we then estimate the expected $F_\nu(u - band)$, the modelled flux density in the *u* band, assuming zero flux below 912 Å (i.e. $f_{esc}(\mathrm{LyC}) = 0.0$). This value is taken as the weighted average of the composite spectrum, redshifted based on the observed redshift from our MOSFIRE emission lines, where the weights are given by the *u*-band sensitivity. This weighting takes into account the CLAUDS *u* transmission curve, the detector quantum efficiency (QE), optical throughput of the telescope/instrument, and atmospheric transmission. The resulting transmission curve is shown as a cyan dashed line in Fig. 5, and shows that including these additional effects (QE in particular) produces a strong weighting towards the redder portion of the filter (compare to the filter-only transmission in Fig. 1). As the red portion of the filter contains the Lyα forest contribution, accounting for the full system response is critical in accurately estimating f_{esc}(LyC).

After computing the expected $F_\nu(u - \mathrm{band})$ assuming $f_{esc}(\mathrm{LyC}) = 0.0$, we then compare this to the observed value from CLAUDS photometry indicated by the red, dashed line in Fig. 5. For three galaxies, the modeled $F_\nu(u - \mathrm{band})$ for $f_{esc}(\mathrm{LyC}) = 0.0$ is lower than the observed value. This indicates that additional flux, beyond what is contained in the Lyα forest, is required in the *u* band to match the photometric observations (i.e. F_ν(LyC)). We show the observed $F_\nu(u - \mathrm{band})$ in Fig. 5 using the red dashed line. We note here that, due to the low sensitivity to LyC photons in the *u*-band observations (indicated by the sensitivity curve in Fig. 5), the modelled values here may be somewhat underestimated.

For cases where additional flux is required in our composite spectrum to match the observed $F_\nu(u - \mathrm{band})$, we then iteratively add flux to the composite spectrum at $\lambda_{rest} < 912$ Å until the modeled $F_\nu(u - \mathrm{band})$ matches the observed value. This added flux in the LyC region is added simply as a flat distribution in $F_\nu(\lambda)$ over *u*-band wavelengths where the amount of flux added in each iteration is equal to 0.01 times the observed $F_\nu(UV)$. Thus, our estimate of $F_\nu(\mathrm{LyC})/F_\nu(UV)$ has a precision of 0.01, which we find equates to an f_{esc}(LyC) precision significantly smaller than the corresponding error due to uncertainty in the photometric measurement.

In cases where no additional flux is required to match the observed $F_\nu(u - \mathrm{band})$, we then estimate the upper limit on f_{esc}(LyC) based on the photometric uncertainty of the CLAUDS *u* band observation. This is done by adding the uncertainty in *u* to the observed value and again comparing to the modeled *u* flux for $f_{esc}(\mathrm{LyC}) = 0.0$. In cases where we still find no additional flux is required, we record an $f_{esc}(\mathrm{LyC}) = 0.0$ for that galaxy. Otherwise, we perform the same iterative process described above, this time using the observed $F_\nu(u - \mathrm{band})$ with the added photometric uncertainty. In such cases, the resulting f_{esc}(LyC) value is taken as an upper limit. The blue composite spectrum in Fig. 5 illustrates the flat F_ν(LyC) required for galaxy 17800 such that the modeled $F_\nu(u - band)$ matches the observed value with the photometric uncertainty added.

Next, we must convert the estimated F_ν(LyC) to f_{esc}(LyC) for each galaxy. To do this requires an assumption regarding the intrinsic LyC to UV luminosity, $(L_\nu(\mathrm{LyC})/L_\nu(UV))_{int}$, and the transmission of LyC through the IGM at the redshift of each galaxy. While there may be some variation in $(L_\nu(\mathrm{LyC})/L_\nu(UV))_{int}$, particularly at high redshift (e.g. Chevallard et al. 2018), we assume a value of 0.33, which is a commonly assumed value in the literature (Steidel, Pettini & Adelberger 2001; Inoue et al. 2005; Shapley et al. 2006; Vanzella et al. 2012). We check how reasonable this value of $(L_\nu(\mathrm{LyC})/L_\nu(UV))_{int}$ is for our sample by estimating the efficiency of ionizing photon production, ξ as:

$$\xi = \frac{N_{\mathrm{LyC}}}{L(UV)}, \tag{5}$$

where $N_{\rm LyC}$ is the production rate of ionizing photons. We calculate $N_{\rm LyC}$ based on the dust corrected Hβ luminosity and the value of $f_{\rm esc}$(LyC) (calculated below):

$$N_{LyC} = 2.1 \times 10^{12} L(\mathrm{H}\beta) \times (1 - f_{\rm esc}(\mathrm{LyC}))^{-1} \quad (6)$$

This follows Izotov et al. (2017) using the values quoted in Storey & Hummer (1995). We note that estimating ξ also requires a slit correction to $L(UV)$ as this photometric value is taken in a circular aperture while H β measurement is performed in a narrow slit. We can roughly estimate this correction by comparing the catalogue value of $F(UV)$ to the value measured in our MOSFIRE slit; however, the true correction may vary if the H β emitting region is not spatially coincident with the UV emitting region (e.g. if H β is more extended, this correction will underestimate ξ). We also note that our attenuation correction for Hβ is based on the UV spectral slope of the stellar continuum light assuming $E(B-V)_{\rm stars} = E(B-V)_{\rm gas}$. If the nebular emission is in fact more attenuated than the stellar light (as is often the case at low z, e.g. Calzetti et al. 1994, 2000), our attenuation-corrected value of L(Hβ), and thus ξ, will be underestimated.

For H β-detected galaxies in our sample, values of log(ξ) vary from 24.44 to 25.07. These values are lower than the canonical value used for theoretical work on the EOR of log(ξ) $\sim$ 25.2–25.3 (e.g. Robertson et al. 2013), but are comparable to low H β(EW) compact star-forming galaxies at low redshift from Izotov et al. (2017). Estimating H β EW for our sample for comparison is not possible though as our MOSFIRE spectra are not continuum-detected. Compared to samples in the redshift range $1.4 < z < 2.2$, our measurements of ξ are lower than average, but overlap with the low ξ end of observed galaxies (e.g. Matthee et al. 2017; Shivaei et al. 2018). Nakajima et al. (2016) estimate ξ for LAEs at $3.1 < z < 3.7$, a similar redshift to our sample, finding log(ξ) > 25 for H β-detected galaxies. Upper limits for H β non-detected galaxies from Nakajima et al. (2016), however, are consistent with the values computed for our sample. At $z > 4$, typical ξ measurements are significantly higher than our sample (Bouwens et al. 2016; Stark et al. 2015, 2017).

What may be the cause of our apparent bias of our sample towards low ξ galaxies? A complex/bursty star-formation history and/or a significant old stellar population in our sample could explain such low values of ξ. Such a complex star-formation history may be reasonable given the relatively large stellar masses of our sample. Related to this, it has been suggested that ξ may be inversely correlated with stellar mass with more massive galaxies having a lower production of ionizing photons (e.g. Faisst 2016; Matthee et al. 2017), consistent with the low values found for our sample. Finally, we note that the value of ξ calculated here depends directly on $f_{\rm esc}$(LyC), which itself depends on the assumed ξ. Regardless, we adopt a value of $(L_\nu(\mathrm{LyC})/L_\nu(UV))_{\rm int}$ of 0.33 to compare directly with other studies. A lower value of ξ corresponds to a lower value of $(L_\nu(\mathrm{LyC})/L_\nu(UV))_{\rm int}$ and, in turn, this would result in a *higher* estimate of $f_{\rm esc}$(LyC). Thus, values quoted here should be considered conservative in this sense.

As for the IGM transmission of LyC, $T_{\rm IGM}$(LyC), for each galaxy we reproduce the average IGM transmission curves at the redshift of the galaxy following the analytic functions provided in Inoue et al. (2014) and apply the modelled value at 912 Å. We then compute the *relative* LyC escape, $f_{\rm esc,\,rel}$(LyC), from our photometric measurements as:

$$f_{\rm esc,rel}(\mathrm{LyC}) = \frac{F_\nu(\mathrm{LyC})}{F_\nu(UV)} \times \left(\left(\frac{L_\nu(\mathrm{LyC})}{L_\nu(UV)} \right)_{\rm int} T_{\rm IGM}(\mathrm{LyC}) \right)^{-1} \quad (7)$$

We must then apply a dust correction to the UV luminosity to compute the absolute $f_{\rm esc}$(LyC) following (Inoue et al. 2005; Siana et al. 2007):

$$f_{\rm esc}(\mathrm{LyC}) = f_{\rm esc,rel}(\mathrm{LyC}) \times 10^{-0.4 A_{UV}} \quad (8)$$

where A_{UV} is the dust attenuation at 1500 Å evaluated for an SMC attenuation curve (Gordon & Clayton 1998) with $E(B-V)$ from the UV slope as measured in Section 4.2 (see Table 2).

Due to the stochastic nature of the column density of neutral hydrogen in any one sightline through the IGM, the adopted value *T*IGM(LyC) represents the largest uncertainty for individual estimates of $f_{\rm esc}$(LyC). Modelled values of $f_{\rm esc,\,rel}$(LyC) and $f_{\rm esc}$(LyC) for each galaxy are quoted in Table 3 and we compare these values with O32 ratios in Section 6.3. Upper and lower limits on $f_{\rm esc}$(LyC) are taken by evaluating $f_{\rm esc}$(LyC) using the above methodology with the photometric uncertainty added or subtracted from the observed value. We note that in most cases subtracting the photometric uncertainty results in the u mag consisted with $f_{\rm esc}(\mathrm{LyC}) = 0.0$. Summarizing our assessment of LyC escape in our sample, 3/8 galaxies have u band flux consistent with $0.07 < f_{\rm esc}(\mathrm{LyC}) < 0.37$, 2/8 have upper limits on $f_{\rm esc}$(LyC) of 0.04 and 0.06, and the remaining 3/8 have u-band photometry consistent with $f_{\rm esc}(\mathrm{LyC}) = 0.0$.

Although we have obtained LRIS spectra for each galaxy, we defer estimating $f_{\rm esc}$(LyC) from these spectra to future work (Meštrić et al. in preparation) due to the low signal to noise (*S/N*) of these spectra. In the LyC region of our LRIS spectra we obtain an average *S/N* of $\sim$0.2 per pixel and LyC emission is also often affected by individual noise spikes in our spectra as seen in Fig. 5. Future work, relying on an advanced flat-fielding technique and stacking analysis of our larger sample of LRIS observed galaxies, will provide spectroscopic measurements of the average $f_{\rm esc}$(LyC) of u-band selected targets (Meštrić et al. in preparation).

Table 3. Estimates of $f_{\rm esc}$(LyC) and Lyα EW.

ID	$f_{\rm esc,\,rel}(\mathrm{LyC})^a$	$f_{\rm esc}(\mathrm{LyC})^b$	Lyα EW^c
12676	$\leq$0.09	$\leq$0.04	–
13459	0.0 ± 0.0	0.0 ± 0.0	–
14528	0.0 ± 0.0	0.0 ± 0.0	104 ± 35
15332	$0.12^{+0.26}_{-0.12}$	$0.07^{+0.14}_{0.07}$	50 ± 11
15625	0.0 ± 0.0	0.0 ± 0.0	20 ± 5
16067	$\leq$0.09	$\leq$0.06	58 ± 11
17251	0.81 ± 0.16	0.37 ± 0.08	26 ± 8
17800	0.29 ± 0.13	0.21 ± 0.09	–

Note. [a]estimated from CLAUDS u-band photometry.
[b]absolute $f_{\rm esc}$(LyC) after applying dust correction (SMC) to $f_{\rm esc,\,rel}$(LyC).
[c]Rest-frame Lyα equivalent width for Lyα emitters only.

5 RESULTS

5.1 Rest-frame optical emission line ratios

In this section, we present optical emission line ratios for galaxies with clean detections of [O II] ($\lambda\lambda$3727 Å), [O III] (λ4959 Å), and [O III] (λ5007 Å) in comparison with samples of highly ionized galaxies at both low- and high-redshift. In particular, we examine

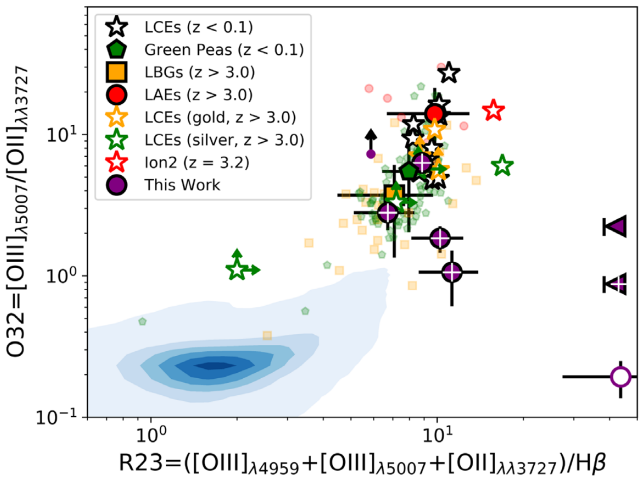

Figure 6. R23 vs O32 for our sample in comparison with various samples of high- and low-redshift star-forming galaxies. For most comparison samples, small symbols indicate individual galaxies and corresponding large, opaque symbols show averages for each sample. The exception is LyC emitting galaxies shown as white stars. Those with black edges are low-z galaxies from Izotov et al. (2016), Izotov et al. (2018a), and Izotov et al. (2018b), the red edged white star is the high-z galaxy Ion2 (de Barros et al. 2016; Vanzella et al. 2016), and orange- and green edged white stars are $z > 3.0$ galaxies from the 'gold subsample' and 'silver subsample', respectively, of the LACES survey (Fletcher et al. 2018). Star-forming SDSS galaxies from (Zahid et al. 2013) are shown by the blue density contours. Galaxies in our MOSFIRE sample with detections of [O II] (λλ3727 Å), [O III] (λ4959 Å), [O III] (λ5007 Å), and H β are shown with large purple circles. Circles with white crosses indicate confirmed Ly α emitters. Filled triangles represent those galaxies without H β observations indicating only O32 values and not R23 upper-limits. The small purple circle indicates the upper limit on O32 for galaxy 13459 (not detected in [O II] λλ3727 Å). The open purple circle represents galaxy 17251, which shows evidence of being an ongoing merger (see Fig. 2 and Section 5.1.1). Shocks associated with mergers may explain both the high R23 and low O32 values observed in this galaxy.

the line ratios:

$$R23 = \frac{[O\,\mathrm{ii}]_{\lambda\lambda3727} + [O\,\mathrm{iii}]_{\lambda4959} + [O\,\mathrm{iii}]_{\lambda5007}}{H\beta} \quad (9)$$

and

$$O32 = \frac{[O\,\mathrm{iii}]_{\lambda5007}}{[O\,\mathrm{ii}]_{\lambda\lambda3727}}. \quad (10)$$

R23 has long been suggested as an indicator of the physical conditions of H II regions in star-forming galaxies (Pagel et al. 1979). More recently, a comparison between R23 and O32 has been used in studies of high ionization in star-forming galaxies (e.g. Nakajima & Ouchi 2014) as O32 is sensitive to the ionization state of star-forming gas (Kewley & Dopita 2002; Steidel et al. 2014, 2016). Our results are presented in Fig. 6.

As discussed in Section 4.1, among our selected sample of eight galaxies at $\langle z \rangle = 3.17$, five were well detected in [O II] (λλ3727 Å), [O III] (λ4959 Å), [O III] (λ5007 Å), and H β. Of the remaining three, two were only detected in [O II] (λλ3727 Å), [O III] (λ4959 Å), and [O III] (λ5007 Å), and the third was detected in [O III] (λ4959 Å), [O III] (λ5007 Å), and Hβ. For this latter object (galaxy 13459) we include an upper limit on [O II] (λλ3727 Å), but do not include limits on Hβ for the former two (12676 and 14528) for reasons described in Section 4.1 (and see Fig. 3). It has been suggested by recent works (e.g. Izotov et al. 2018b) that only O32 may be required to provide an estimate of f_{esc}(LyC) (see also Sections 5.2 and 6.3), thus we can make an additional estimate of f_{esc}(LyC) independent of u band photometry even for those galaxies with no Hβ detection.

The resulting R23 vs O32 values for five galaxies with detections in all lines are shown as purple circles in Fig. 6. The five galaxies in our sample that are also found to be Lyα emitters from our LRIS observations are indicated with white crosses. Four out of five galaxies well detected in all lines are found to have a large average value of O32 $\gtrsim 1.0$, consistent with a high ionization parameter. Lyα emitters are found to cover the full range in O32 ratios observed in our sample, though the strongest Lyα emitter in our sample also has the highest O32 of 6.3 ± 0.7 (excluding the lower limit for 13459). The fifth galaxy from our sample observed in all five lines (17251), shown with an open purple circle, exhibits an R23 value inconsistent with pure photoionization as we describe in Section 5.1.1.

Galaxy 13459, which is not detected in [O II] (λλ3727 Å), is shown as a small purple circle with an upward arrow indicating this as a lower limit on O32. This galaxy also has a high O32, indicating high ionization similar to other galaxies in our sample. Such a large O32 also means that the effect of [O II] (λλ3727 Å) emission on the observed value of R23 will be negligible.

The two galaxies from our observations without a clear detection of H β are plotted as filled purple triangles in Fig. 6. H β for these observations either fell below the wavelength coverage of our observations or overlapped with a strong skyline (see Fig. 3), preventing our measurement. Thus, the solid purple triangles do not represent a limit on R23, as this is entirely unknown, but simply serve to indicate their O32 ratio. These two galaxies are found at large O32 with values of 0.9 ± 0.1 and 2.2 ± 0.3, in the same range as for previously discussed galaxies.

Fig. 6 also displays comparison samples of low redshift, star-forming galaxies. Blue density contours represent 51 262 star-forming galaxies from the Sloan Digital Sky Survey (SDSS) from Zahid et al. (2013), and are representative of the bulk of low redshift, star-forming galaxies. So called 'green' galaxies (Cardamone et al. 2009) are a well-studied population of compact and highly star-forming low redshift galaxies. Those presented in Fig. 6 are a compilation from Yang et al. (2016) and Cardamone et al. (2009) galaxies that overlap with the Zahid et al. (2013) sample. Compared to the bulk of galaxies from Zahid et al. (2013), green peas are highly ionized, with average O32 values larger than 1.0, comparable to our sample.

In addition to the low redshift comparison samples, we also show in Fig. 6 two redshift ∼3-4 samples, typical of star-forming galaxies at this epoch. These are LBGs compiled from Troncoso et al. (2014) and Maiolino et al. (2008) and LAEs taken from Nakajima & Ouchi (2014) and Nakajima et al. (2016). LBGs closely overlap the distribution of green peas whereas LAEs from the literature are typically found at the highest O32 among all samples in Fig. 6.

Our MOSFIRE sample is wel-matched to the upper end of the O32 distribution for LBGs while falling below the O32 values of LAEs. This is not surprising as the $(g - r)$ vs $(u - g)$ colours of our sample are consistent with the standard LBG selection (e.g. Steidel et al. 1996). It is interesting to note that, although LAEs from the literature are found at the very high end of the O32 distribution, the five galaxies in our MOSFIRE sample that are also found to emit Lyα (black crosses) extend this sample to lower O32. This is perhaps not surprising given that Shapley et al. (2003) find that roughly half of the LBGs in their sample exhibit some Ly α in emission. Unlike Shapley et al. (2003), 62.5 per cent of our selection exhibit Ly α emission, and these emitters have Ly α EW > 20 Å. Ly α emission of this strength only occurs in ∼25 per cent of the Shapley et al. (2003)

sample. We also consider the 13/15 LCE's presented in Steidel et al. (2018) exhibit Lyα in emission, however only 4/15 (26.7 per cent) have Lyα EW > 20 Å. This may suggest that selecting $z \sim 3$ LBGs with high *uS* fluxes may preferentially select those with high Ly α EW, though not exclusively. These results highlight the fact that LAEs and LBGs are likely drawn from the same general parent sample of high redshift, star-forming galaxies, while their observed properties simply reflect the differing methods of selection.

A key comparison for our sample in terms of f_{esc}(LyC), are confirmed LCEs. Low redshift LCEs taken from Izotov et al. (2016), Izotov et al. (2018b), and Izotov et al. (2018a) are shown as open black stars. These galaxies are selected from a parent sample of green peas based both on their compactness and their large O32 values. All nine of these galaxies are found to have O32 > 4.0, and, in particular, the three strongest LCEs with $f_{esc}(\mathrm{LyC}) = 0.38 - 0.73$, are among the galaxies with the highest O32 values in the range 11.5–16.3. The remaining low-redshift LCEs are found to have $f_{esc}(\mathrm{LyC}) \leq 0.14$.

Also shown in Fig. 6 as open red, orange, and green bordered stars are known samples of $z > 3.0$ LCEs also having measurements of O32. The red bordered star is the galaxy 'Ion2' (de Barros et al. 2016; Vanzella et al. 2016) and the orange bordered stars are 'gold subsample' galaxies from the LACES survey having measurements of R23 and O32 (Fletcher et al. 2018). LACES 'silver subsample' galaxies, which have lower *S/N* detections of LyC, are shown with green bordered stars, however 3/4 have only lower limits on both R23 and O32. We also exclude one LACES silver galaxy (galaxy 94460) as they note their spectroscopic observations indicate possible low redshift contamination. The LACES gold and silver subsamples include six and four additional LCEs, respectively, without optical line ratios. It should also be mentioned that all LACES LCEs are found to also be Ly α emitters with Ly α EW > 20, similar to Ly α emitters in our sample. All high-redshift LCEs from the literature in Fig. 6, excluding lower limits, have O32 > 5.6, with Ion2 found at the highest O32 of 14.7.

Taken together, the combined sample of high- and low-redshift LCEs with O32 measurements suggest that high ionization, as indicated by a high O32, is a possible identifying feature of LyC escape from star-forming galaxies. It should be noted, however, that the galaxy with the largest O32 value from Izotov et al. (2018a) of 27.2 has a relatively low estimated f_{esc}(LyC) value of 0.11. We discuss the possible connection between observed values of O32 and f_{esc}(LyC) further in Section 6.3.

Among our six galaxies with reliable O32 measurements, one has O32 matching the O32 range exhibited by LCEs. As we have described, the estimated f_{esc}(LyC) for these low O32 LCEs is of the order or 0.05–0.17. High-redshift LCEs also seem to follow similar trends between O32 and f_{esc}(LyC) seen by Izotov et al. (2018b). As we will see in Section 6.3, the empirical relationship between O32 and f_{esc}(LyC) from Izotov et al. (2018b) and Faisst (2016) predicts an f_{esc}(LyC) of 0.10-0.16 for galaxy 16067, our galaxy having the largest O32 value among those detected in [O II] (λλ3727 Å). This f_{esc}(LyC) for galaxy 16067 is in roughly 2× larger than the upper limit on f_{esc}(LyC) estimated from CLAUDS *u* band photometry quoted in Table 3. Furthermore, as mentioned in Section 4.1, the [O II] (λ3729 Å) flux for gal'axy 16067 is contaminated by OH emission and likely overestimated as indicated by the implausibly large [O II] doublet ratio (λ3729 Å/λ3726 Å). The suggests an underestimate of O32 that, if true, would imply a larger discrepancy between the predicted f_{esc}(LyC) (from O32) and the observed value (from *u*-band photometry). In addition, we estimate a lower limit for O32 of 8.51 for galaxy 13459 corresponding to $f_{esc}(\mathrm{LyC}) > 0.22$ based on the relation of Izotov et al. (2018b). Interestingly, this galaxy is a non-detection in our CLAUDS *u* band image (though a bright, likely low redshift, *u* band source can be seen in the cutout shown in Fig. 2), and thus consistent with $f_{esc}(\mathrm{LyC}) = 0.0$.

From O32 alone, the remaining galaxies are expected to be negligible emitters of LyC photons (though we estimate f_{esc}(LyC) from *u*-band photometry as high as 0.07–0.37 for some of these galaxies, see Sections 4.4 and 6.3). We note that galaxies in this pilot survey were selected as bright, and thus likely more massive and less compact compared to Ion2 and green peas, which may bias us to a sample with lower O32 (and thus lower f_{esc}). See Section 6.1 for more discussion of this. A final caveat is that, although all confirmed LCEs are found at high O32, the value of O32 for other samples of high redshift LCEs are currently unknown (e.g. Steidel et al. 2018).

5.1.1 *Galaxy 17251*

Galaxy 17251 is plotted with an open, purple circle was found to have an extremely large R23 value of 43.8, which is roughly five times higher than the average value for galaxies in our sample with reliable H β detections. This large value is also at odds with theoretical expectations from photoionization modelling, which give an upper bound of ∼10 (Kewley & Dopita 2002; Nagao, Maiolino & Marconi 2006). Examining the 2D spectra from MOSFIRE, we find significant velocity structure in the [O III] (λ5007 Å) emission line as shown in the boxcar smoothed (kernel width = 1 pixel) cutout in Fig. 7. The primary galaxy is located at emission peak A while peaks B and C are found to have velocity offsets for the [O III] (λ5007 Å) emission line of +38 and + 52 km s^{-1} respectively. We indicate the average seeing of our K-band observations of 0.″79 with a white scale bar, a size comparable to peaks B and C. Thus, the size of these structures is consistent with the seeing FWHM, thus, they are likely real but only marginally resolved in our MOSFIRE observations.

This complex structure may be indicative of an ongoing merger, a possibility consistent with the irregular morphology seen in the HST image shown in Fig. 2. We reextracted the spectra in narrow spatial apertures in an attempt to capture the properties of the individual emission line regions. We find that region A and C have similar values of [O III]/Hβ of 9.6 and 7.8, respectively. This may be due to the fact that there is significant spatial overlap between these regions in the 2D spectrum making it difficult to extract a spectrum for region C with no contribution from region A. Region B is found to exhibit no measurable Hβ emission and relatively weak [O III] (λ5007 Å) emission.

Shocks, which are common in ongoing galaxy mergers, are known to have strong effects on emission line ratios (e.g. Rich, Kewley & Dopita 2015), and in particular can greatly enhance [O II] (λλ3727 Å) emission relative to [O III] (λ 5007 Å) and Hβ (Epinat et al. 2018). This could help to explain both the high R23 and the low O32 found for this galaxy. The poorer seeing of our H-band observations (0.96 arccsec versus 0.79 arcsec for the K-band) as well as contamination from sky emission lines prevent us from performing a similar extraction of spectra for individual emission line peaks for [O II] (λ3727 Å) emission to test this. Regardless, the fact that shocks associated with merger activity can significantly impact the observed line ratios is important in the comparison between f_{esc}(LyC) and O32 both here and in all O32 studies of LCEs.. This is particularly interesting as we estimate $f_{esc}(\mathrm{LyC}) = 0.37$ for this galaxy from photometry.

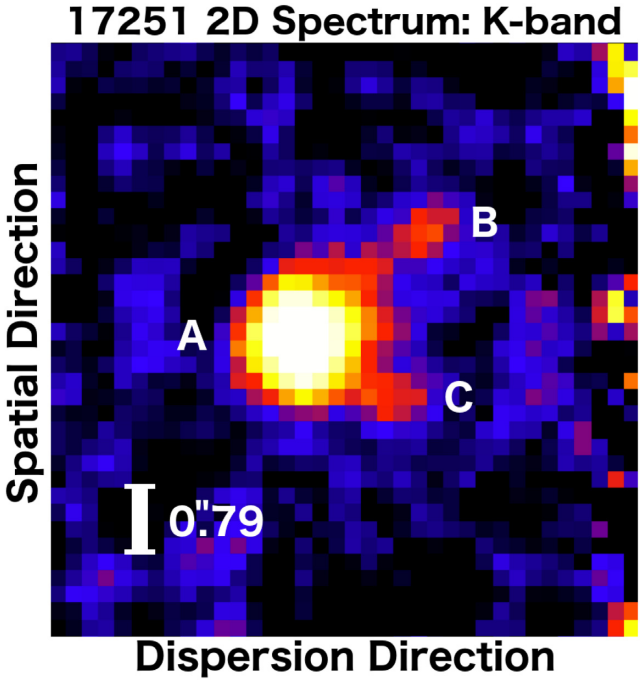

Figure 7. A cutout of the region in the 2D MOSFIRE, K-band spectrum of galaxy 17251 smoothed using a boxcar kernel with a width of 1 pixel. This galaxy is found to have significant velocity structure with emission in regions B and C estimated to have velocity offsets of +52 and + 38 km s^{-1}, respectively, from the primary galaxy denoted as region A. Both regions B and C have sizes comparable to the 0.79 arcsec seeing of our observations (indicated by the white scale bar), meaning they are only marginally resolved. This complex structure may be indicative of an ongoing merger, which could account for both the large value of R23 (43.8) and the small value of O32 (0.2), as [O II] (λλ3727 Å) emission is known to be enhanced by shocks in regions between merging galaxies (e.g. Epinat et al. 2018).

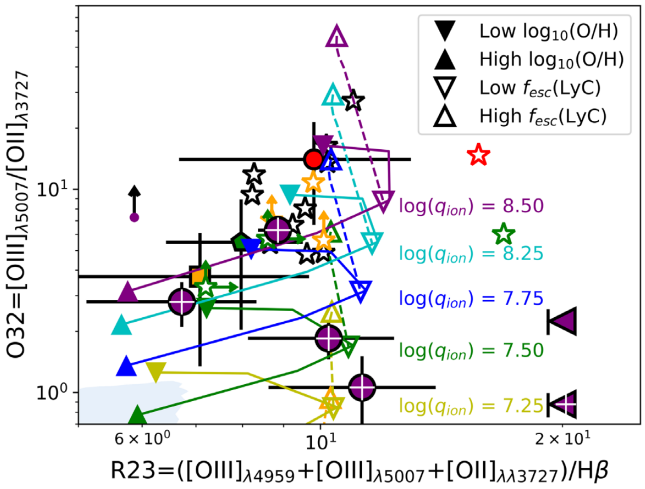

Figure 8. R23 versus O32 diagram, similar to Fig. 6, however, now we have zoomed into the upper-right region where highly ionized galaxies are found. With the exception of LCEs (white stars), individual galaxies in comparison samples have been removed for simplicity. Symbols common to both figures are the same as in Fig. 6. The major addition in this figure are photoionization modelling tracks output by the MAPPINGS V code. Solid lines show tracks for ionization-bounded models of constant ionization parameter, $q_{\rm ion}$ (values shown in the annotated text with corresponding colours), with increasing $12 + \log_{10}(O/H)$ as indicated by the filled triangles. Dashed lines show tracks with increasing $f_{\rm esc}$(LyC), as indicated by the open triangles, at fixed $q_{\rm ion}$ and $12 + \log_{10}$(O/H). These models clearly show the three-fold degeneracy between $q_{\rm ion}$, $12 + log_{10}$(O/H), and $f_{\rm esc}$(LyC) in the observed R23-O32 space.

5.2 Comparison with photoionization modelling

Here we present the emission line ratios calculated in our photoionization models, described in Section 4.3. Separate metallicity and $f_{\rm esc}$(LyC) tracks in R23 vs O32 at fixed ionization parameter, $q_{\rm ion}$, are shown in Fig. 8. Solid lines represent ionization bounded models ($f_{\rm esc}$(LyC) = 0.0) at various metallicities, whereas dashed lines represent density bounded models at a fixed metallicity from $f_{\rm esc}$(LyC) = 0.0 to $f_{\rm esc}$(LyC) = 1.0. Tracks are shown over observed values for our sample, as well as average values for comparison samples described in Section 5.1.

Results presented for ionization bounded models in Fig. 8 mirror those presented in Nakajima & Ouchi (2014). This is not surprising as R23 vs O32 tracks from Nakajima & Ouchi (2014) were based on values from a previous version of the MAPPINGS code presented in Kewley & Dopita (2002). The key point illustrated by these ionization bounded models is a clear degeneracy between metallicity and $q_{\rm ion}$. Nakajima & Ouchi (2014) show that, by using an iterative process, an estimate of gas-phase metallicity, $12 + \log_{10}$(O/H), and $q_{\rm ion}$ can be calculated based on the solid curves in Fig. 8. Following the example of Nakajima & Ouchi (2014), we also calculate $q_{\rm ion}$ and $12 + \log_{10}$(O/H) finding values in the range $7.67 < q_{\rm ion} < 8.10$ and $8.18 < 12 + log_{10}(O/H) < 8.86$. Nakajima & Ouchi (2014) show that these are similar to the average values for green peas and LBGs.

Also shown in Fig. 8 as dashed lines are tracks for density bounded photoionization models calculated as described in Section 4.3. Each track is calculated at a fixed metallicity of $12 + \log_{10}(O/H) = 8.48$ with $f_{\rm esc}$(LyC) increasing from 0 to 1.0. As expected, the $f_{\rm esc}$(LyC) = 0.0 model overlaps the ionization bounded model at the corresponding $q_{\rm ion}$ and metallicity, while nonzero $f_{\rm esc}$(LyC) models extend to higher O32 with little variation in R23.

Ionization and density bounded models in Fig. 8 demonstrate the threefold degeneracy between metallicity, ionization parameter, and $f_{\rm esc}$(LyC) in the R23 vs O32 plane. Clearly, for LyC emitting galaxies, an iterative approach in calculating ionization parameter and metallicity based on R23 and O32 (e.g. Nakajima & Ouchi 2014), where an ionization bounded model has been assumed may not be applicable.

Of course, the comparison here is between ionization and density bounded models with simple geometry. In cases where LyC photons escape through holes in geometrically complex H II regions, it is still unclear if either of these approximations (density bounded versus ionization bounded) can be applied to integrated line flux measurements (see also discussion in Fletcher et al. 2018; Steidel et al. 2018). As we have noted, the majority of galaxies in our sample have O32 values suggestive of a negligible $f_{\rm esc}$(LyC). Thus, the three low O32 galaxies with accurate R23 values are estimated in the ranges $8.18 < 12 + \log_{10}(O/H) < 8.86$ and $7.67 < \log_{10}(qion) < 7.76$. Although there is a clear degeneracy between metallicity, $q_{\rm ion}$, and $f_{\rm esc}$(LyC), there is also evidence of an empirical trend between metallicity and $q_{\rm ion}$ (e.g. Dopita et al. 2006; Sanders et al. 2016; Onodera et al. 2016; Kojima et al. 2017) that may alleviate some difficulty. We discuss theoretical and empirical trends between $f_{\rm esc}$(LyC) and O32 further in Section 6.3.

6 DISCUSSION

In this work, we have selected eight galaxies that are likely emitters of LyC at $\langle z \rangle = 3.17$ based on their restframe UV colours indicative of LyC emission (as detected in the *uS* band, see Section 2.1), and explored their rest-frame optical emission line properties using spectra from MOSFIRE H- and K-band observations. We have shown in Sections 5.1 that the O32 values found in our selected sample are comparable to other samples of star-forming galaxies at $z > 3.0$, as well as highly ionized galaxies (including confirmed LCEs) at low-redshift.

In this section, we examine the integrated properties of galaxies in our sample, including photometrically estimated f_{esc}(LyC), in comparison to samples of suspected (and confirmed) LyC emitters at high- and low-redshift. This can give a better indication of the likelihood of LyC escape from these galaxies in lieu of spectroscopic LyC detections. In the future, we will compare this analysis with LyC detections (or upper limits) from our LRIS observations and f_{esc}(LyC) measurements from photometry and spectroscopy of higher redshift targets (Cooke et al. in preparation, Meštrić et al. in preparation). In Section 6.2, we discuss how lessons learned from this pilot study have refined our selection methodology with the aim of improving our efficiency of selecting LyC emitters from photometric data and enabling an unbiased investigation of the full $z \sim 3-4$ galaxy population. Finally, in Section 6.3, we discuss the implications of the density bounded photoionization models from 5.2 in comparison with the recent empirical relationship between O32 and f_{esc}(LyC).

6.1 Do photometric LCE candidates represent key contributors to reionization?

In Fig. 9, we explore the relationship between the O32 ratio and M_*, SFR, and sSFR for galaxies in our sample as well as those in comparison samples shown in 'Fig. 6. Green pea galaxies from Yang et al. (2016) and Cardamone et al. (2009) and LCE galaxies from Izotov et al. (2016) and Izotov et al. (2018a) have had their stellar masses and SFRs converted from the Salpeter (1955) IMF used in these studies to the Chabrier (2003) IMF used in this work using conversion factors found in the literature (e.g. Kennicutt & Evans 2012; Speagle et al. 2014). These conversions are largely negligible, however, and have no appreciable effect on our results. Stellar masses and SFRs of high-redshift comparison samples all adopt a similar IMF to ours, thus requiring no adjustment.

Fig. 9 provides a rough assessment of the likelihood that our selected galaxies are significant emitters of LyC photons. Compared with other samples shown in Fig. 9, galaxies in our sample are relatively uniform in M_*, but exhibit a wide spread in the value of O32. In terms of both M_* and SFR, our sample is most similar to intermediate mass green pea galaxies and low mass, but bright, LBGs. We note that here M_* comes from SED fitting where nebular emission lines have been included in the fit as it has been shown that failing to do so results in an overestimate of M_* (e.g. Forrest et al. 2017).

The key comparison with our sample in Fig. 9 is with confirmed LCEs. Considering M_*, 12/16 LCEs are found th have masses one to two orders of magnitude less than the majority of galaxies in our sample. This is consistent with hydrodynamical simulations that find f_{esc}(LyC) significantly decreases with increasing stellar mass (Yajima et al. 2011; Wise et al. 2014). The most massive LCEs from Izotov et al. (2018b), Izotov et al. (2018a), and Fletcher et al. (2018) have comparable mass to our sample and overlap in O32 with our highest O32 galaxies. Furthermore, the SFRs of galaxies in our sample overlap with the high SFR end of LCEs. Assuming these galaxies form stars from a similar initial mass function, this would imply comparable numbers of massive stars and, thus, a similar production rate of ionizing photons. The caveat here is that, as we estimated in Section 4.4, galaxies in our sample may in fact have a low efficiency of ionizing photon production, ξ (although our estimate is highly uncertain due to unknown effects of slit-loss). Considering sSFR we find again that galaxies in our sample are comparable to those found for LCEs. We note again that hydrodynamical simulations find a correlation between increasing sSFR and increasing f_{esc}(LyC) (Yajima et al. 2011; Wise et al. 2014).

We recall the fact that 5/8 of the galaxies in our sample exhibit confirmed Ly α emission from our LRIS observations. Similarly, the vast majority currently confirmed detections of LyC emission from spectra occur in galaxies also exhibiting Lyα emission (Heckman et al. 2011; Leitet et al. 2013; de Barros et al. 2016; Izotov et al. 2016, 2018a,b; Leitherer et al. 2016; Shapley et al. 2016; Vanzella et al. 2016, 2017; Fletcher et al. 2018; Steidel et al. 2018). We note that the Lyα properties of the redshift ∼2.5 LCE from Bian et al. (2017) are unknown as this galaxy lacks spectroscopic observations targeting the Lyα wavelength range. Regardless, there appears to be a connection between Lyα and LyC escape with Verhamme et al. (2017) showing that $f_{esc}(Ly\alpha)$ is correlated with f_{esc}(LyC) at low redshift. Furthermore, Izotov et al. (2018b) and Izotov et al. (2018a) show a correlation between f_{esc}(LyC) and the separation of red and blue peaks of the double peaked Lyα line in low-redshift LCEs. Interestingly, our second strongest LCE, galaxy 17800 with $f_{esc}(Lyc) = 0.21 \pm 0.09$ exhibits Lyα in absorption. Additionally, galaxy 12676, which we estimate a non-zero upper limit on f_{esc}(LyC) of 0.04 is also an Ly α absorber. For the remaining three LCEs in our sample, the resolution of our LRIS observations is not sufficient to resolve any possible double peak of the observed Lyα emission lines and thereby test the prediction of Verhamme et al. (2017) at high-redshift.

O32 measurements for our sample allow us to assess the applicability of an O32-f_{esc}(LyC) relation to our sample. The 3 galaxies in our sample that have nonzero estimates of f_{esc}(LyC) based on CLAUDS u and r' band photometry and the two additional galaxies with non-zero upper limits on f_{esc}(LyC) (see Section 4.4) are indicated in Fig. 9 using coloured edges. Symbols with blue edges are firm detections while those with red edges indicate upper limits based on the photometric uncertainty of the CLAUDS u-band observations. Though not detected in [O II] (λλ3727 Å), the lower limit of O32 for galaxy 13459 of 8.5 is larger than any other galaxy in our sample, and this galaxy has u band flux consistent with $f_{esc}(\text{LyC}) = 0.0$. The highest O32 observation for [O II] (λλ3727 Å) detected galaxies is galaxy 16067, for which we estimate a relatively low upper limit on f_{esc}(LyC) of 0.06. We reiterate here that the [O II] (λλ3727 Å) flux may be overestimated due to OH contamination (see Section 4.1), thus its true O32 may be even higher. Among the three galaxies with firm non-zero measurements of f_{esc}(LyC), only galaxy 17800 has an O32 value significantly higher than 1. Most interestingly, galaxy 17251 has both the highest estimate of $f_{esc}(\text{LyC}) = 0.37 \pm 0.08$ and the lowest O32 of 0.19 ± 0.06. If the measured f_{esc}(LyC) values for our sample are confirmed spectroscopically, this suggests a high O32 is not an absolute requirement for LyC escape from star-forming galaxies.

Taking a closer look at the three low O32 LCEs in our sample, we see that two, 17251 and 17800, have some evidence of merger activity indicated by their complex HST morphologies seen in Fig. 2.

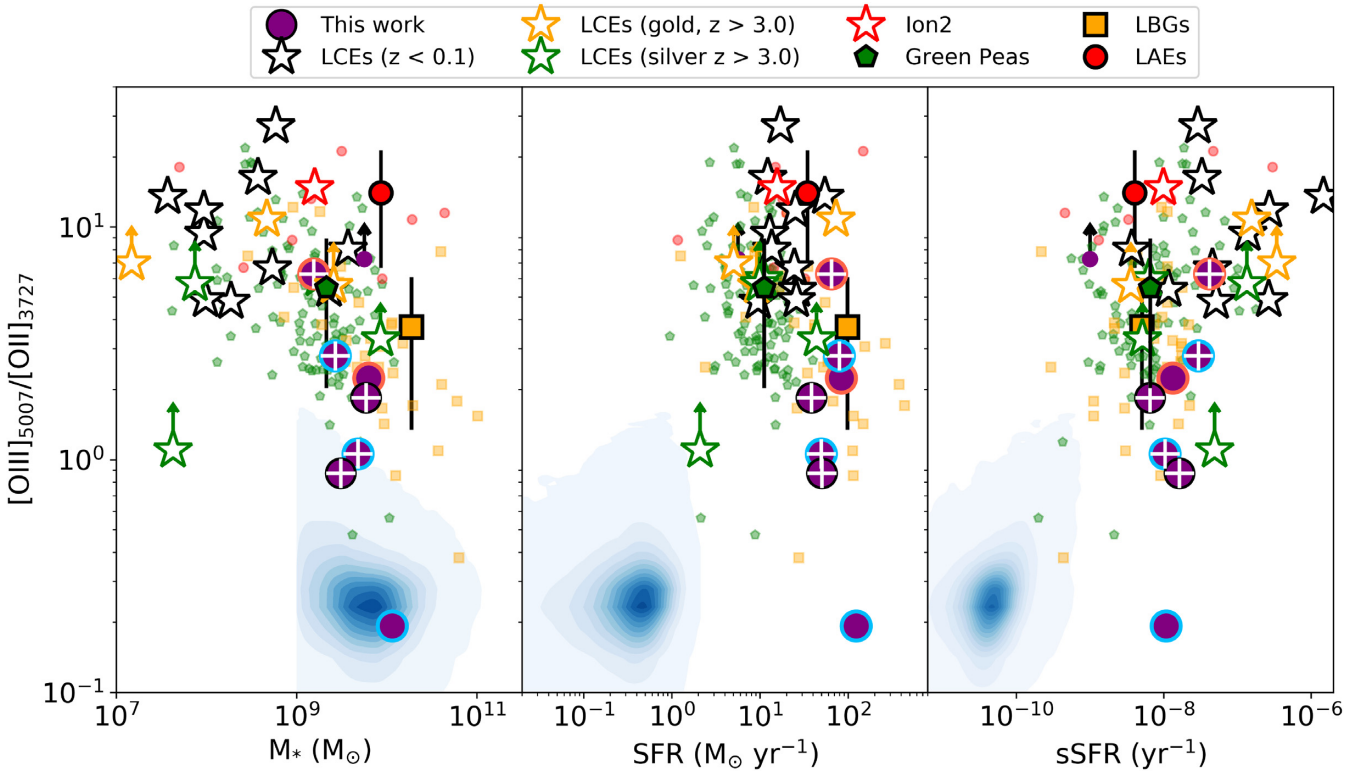

Figure 9. O32 as a function of M_*, SFR, and sSFR for galaxies in our MOSFIRE sample as well as low and high redshift comparison samples. Plotted symbols are the same as in Fig. 6. Purple circles with blue borders indicate the three galaxies having u-band flux consistent with $f_{esc}(LyC) > 0.0$ as estimated in Section 4.4. The two purple circles with red borders indicate galaxies where upper limits on u-band flux provide non-zeros upper limits on $f_{esc}(LyC)$. The remaining three purple circles are galaxies where $f_{esc}(LyC)$ is consistent with zero even within the photometric uncertainty. Galaxies in our sample have M_* comparable to low mass LBGs and high mass green peas, though up to 1 dex more massive than confirmed high-z LCEs. These results are likely reflective of relatively high stellar mass limits imposed for reliable photometric detections at high redshift (i.e. our desire to target bright galaxies). SFRs of our sample are comparable to LBGs, which are typically more star forming than green peas and LCEs. Finally, in terms of sSFR, galaxies in our sample are quite similar to confirmed LCEs.

Galaxy 17251, in particular, which has an extremely low O32, exhibits complex [O III] (λ5007 Å) emission in our 2D spectrum (see Section 5.1.1). It has been shown that the presence of shocks, common in ongoing mergers, can significantly enhance [O II] (λλ3727 Å) relative to [O III] (λ5007 Å), thus reducing the observed O32 (Rich et al. 2015; Epinat et al. 2018). These two high $f_{esc}(LyC)$ galaxies highlight the possibility of a significant role of galaxy mergers in the EoR (see also Bergvall et al. 2013). We discuss further the comparison between O32 and our photometric estimates of $f_{esc}(LyC)$ below in Section 6.3.

The emerging picture of the driver of the EoR is that low mass ($\lesssim 10^8$ $M_\odot$), low luminosity galaxies with high sSFR ($\gtrsim$1 Gyr^{-1}) may be the key sources of reionizing photons (Wise & Cen 2009; Yajima et al. 2011; Wise et al. 2014; Bouwens et al. 2015; Paardekooper et al. 2015). This may relate to the fact that low mass galaxies are smaller in size (e.g. Lange et al. 2015; Bouwens et al. 2017) meaning star-forming regions are more likely to be located near the edge of a galaxy where mechanical star-formation feedback (i.e. supernova blast waves) can more easily reach the IGM. Furthermore, low mass galaxies host less interstellar dust (Garn & Best 2010), meaning LyC emission escaping H II regions is less likely to be attenuated by dust before reaching the IGM in lower mass galaxies.

In this context, given the relatively low $f_{esc}(LyC)$ estimates for the majority of our sample from CLAUDS u-band photometry (which are bright and typically more massive than other known LCEs), we expect that galaxies similar to those selected in this work are not likely to be the key contributors of ionizing radiation during the EoR. Regardless, galaxies such as these will be relevant in estimating the overall ionizing photon budget at $z > 6$. Furthermore, we reiterate that we have estimated a relatively low, though uncertain, value of ξ for our sample (see Section 4.4). If this is reflective of a lower value of $(L_\nu(LyC)/L_\nu(UV))_{int}$, the efficacy of such galaxies to contribute significantly to reionizaion would be further reduced. Finally, it should be stressed that photometric $f_{esc}(LyC)$ estimates presented here are tentative values as LyC photon detections in our LRIS spectra for individual galaxies are still being assessed.

6.2 Improving selections of high-redshift LyC-emitting galaxies

The results of this pilot survey show that the employed selection criteria have not provided a clean sample of $z \simeq 3$ LCEs. In particular, the redshift range probed results in a significant and difficult to distinguish contribution to the u-band photometry from non-LyC photons. This complication means that $f_{esc}(LyC)$ estimates from photometric observations are model dependent, thus prevents us from definitively identifying galaxies in our sample as LCEs.

We also draw attention to the HST imaging for our sample presented in Fig. 2. As we pointed out in Section 2.1, HST morphologies show elongation and/or multiple continuum peaks. These morphological signatures are indicative either of ongoing merger activity, multiple star-forming regions, or line-of-sight contamina-

tion by unrelated, low redshift galaxies. The latter possibility has been shown to prevent a reliable LyC detection (e.g. Vanzella et al. 2010, 2012) as such low redshift contamination would have a strong impact on our *uS* magnitudes. In our sample, no emission lines from lower redshift galaxies are apparent in either our MOSFIRE or LRIS spectra, meaning that our O32 measurements are likely unaffected by any possible low redshift contamination. The one caveat here is that the lack of low redshift emission lines in our MOSFIRE spectrum does not exclude low-redshift, non-star-forming companions that may affect observations of LyC emission. Regardless of the issue of low redshift contamination, our results have shown that ongoing mergers may in fact exhibit heightened LyC escape, thus galaxies with disturbed morphologies should not be avoided entirely.

The challenges and results of this pilot survey have informed and improved our future sample selection of LCE candidates. One goal of our future selection criteria is to avoid both galaxies with $\lambda > 912$ Å emission in *u*-band photometry and galaxies having any possible evidence of low redshift contaminants based on high-resolution HST imaging, though disturbed galaxies indicating possible ongoing mergers are not excluded. This will be achieved by including two additional considerations to our sample selection to improve the efficiency of building our sample of LCEs:

(i) First, we give higher priority to galaxies at $z > 3.4$ with *u* band detections with future selections using the CLAUDS *u* band filter which exhibits a sharp cutoff at 4000 Å, corresponding to 912 Å at $z = 3.4$. We have supplemented this sample with galaxies selected in regions with HST F336W imaging (GO 15100; PI Cooke), which cleanly probes LyC emission down to $z = 3.05$.

(ii) Second, we impose an initial preference for compact galaxies with single UV continuum peaks, and 'clean' detections: those galaxies with no other objects within 1.″0 of the primary source. After this, a secondary preference will be given to galaxies with disturbed morphologies indicative of on-going mergers.

The first criterion allows us to be confident that all photons from $z > 3.4$ galaxies detected in the *u* band are from LyC emission rather than longer wavelength Lyα forest light. This higher redshift cutoff will also aid with spectroscopic detection of LyC photons as the LyC region moves to more sensitive portions of the LRIS CCD. The second criterion ensures we will primarily select galaxies that are the least likely to be affected by lower redshift, line-of-sight interlopers (at the cost of not exploring extended or clumpy galaxies or galaxy mergers). Furthermore, the requirement of compactness follows the work of Izotov et al. (2016) who find that at low-redshift, LCEs are found to be among the most compact galaxies from their parent samples of green peas. On the other hand, our secondary preference for galaxies with disturbed HST morphologies allows us to probe possible galaxy mergers, which we have found in this work to be efficient emitters of LyC radiation. Due to the low covering fraction of primary, compact targets, the inclusion of secondary, disturbed targets further improves the efficiency of our observational strategy.

These selection criteria have been implemented in recent and upcoming observations with LRIS and HST targeting LyC emission, which can provide final confirmation of our selection methodology that has no bias on colour selection or restframe optical emission line strengths. A more complete description of our improved selection criteria and preliminary results of recent HST observations based on this selection will be presented in Cooke at al. (in preparation).

6.3 The correlation between f_{esc}(LyC) and O32

In this section, we discuss the recent suggestion by Faisst (2016) and Izotov et al. (2018b) of an empirical correlation between O32 and f_{esc}(LyC) for galaxies with detected LyC emission. Here, we comment both on the predicted f_{esc}(LyC) for our galaxy sample based on the observed O32 values as well as the comparison with density bounded models computed using the MAPPINGS V code as described in Section 4.3.

The left-hand panel of Fig. 10 compares the observed distribution of confirmed LCEs and the empirical fits in O32 vs f_{esc}(LyC) space while the right panel shows the theoretical predictions of our MAPPINGS V density bounded H II region models. Our fixed metallicity models were calculated on grids with nine values of decreasing H I optical depth, τ_{H1}, simulating f_{esc}(LyC) values from ∼0.999 down to 0.001 and eight values of $\log_{10}(q_{ion})$ from 6.5 to 8.5. We calculated three sets of grids at fixed $12 + log_{10}(O/H)$ of 7.86, 8.48, and 8.99 shown in the right-hand side of Fig. 10 as dotted, dot-dashed, and solid lines, respectively with colours indicating $\log_{10}(q_{ion})$ matched to the values shown in Fig. 8.

At low $12 + log_{10}(O/H)$ and fixed q_{ion} we find that the largest variation in O32 with f_{esc}(LyC) occurs below f_{esc}(LyC) $= 0.10$. For low metallicity models there is still some increase in O32 with increasing f_{esc}(LyC) above f_{esc}(LyC) $= 0.10$, with larger variation at higher ionization. Consider the $12 + \log_{10}$(O/H) $= 8.48$, $\log_{10}(q_{ion}) = 7.75$ model (solid blue line) for instance, from f_{esc}(LyC) =0.01 to f_{esc}(LyC) =0.10, we find an increase in O32 from 3.2 to 11.5. For the same model, however we find between f_{esc}(LyC) =0.10 to f_{esc}(LyC) = 0.75 only a comparatively modest increase in O32 from 11.5 to 14.9. Although we find a more constantly varying f_{esc}(LyC) as a function of O32 for high metallicity and high ionization models (e.g. the purple dot-dashed line in Fig. 10) examples of highly ionized, high-metallicity galaxies are not present in the literature (e.g. Kojima et al. 2017).

Thus, our MAPPINGS V density bounded H II region models suggest that at low metallicity, O32 may have little constraining power on the escape fraction of LyC above f_{esc}(LyC) > 0.10. At high metallicities, O32 may be more predictive of f_{esc}(LyC) with the caveat the MAPPINGS V models are one-dimensional. Fig. 10 clearly shows that an accurate measurement of both metallicity and ionization parameter will be essential in reliably constraining f_{esc}(LyC) from optical emission line ratios alone. Empirically, there is strong evidence that metallicity and ionization parameter are generally correlated (Dopita et al. 2006; Sanders et al. 2016; Onodera et al. 2016; Kojima et al. 2017) and such observations will be vital in obtaining estimates of f_{esc}(LyC) from strong line ratios. Although our MAPPINGS V models presented here, given full freedom in q_{ion} and $12 + log_{10}(O/H)$, can populate the entire O32 vs f_{esc}(LyC) space (thus matching all known LCEs), these empirical results show that certain combinations of metallicity and ionization may be unrealistic.

Low redshift LCEs from Izotov et al. (2016) and Izotov et al. (2018b) are shown by black open stars while more recent observations from Izotov et al. (2018a) are shown with blue open stars. Other low redshift LCEs, with f_{esc}(LyC) measured by Chisholm et al. (2017), are shown with grey circles (Borthakur et al. 2014; Alexandroff et al. 2015; Leitherer et al. 2016). Also shown are $z > 3.0$ LCEs with red, orange and green stars representing Ion2 (de Barros et al. 2016; Vanzella et al. 2016) and 'gold' and 'silver' subsamples from the LACES survey (Fletcher et al. 2018), respectively. f_{esc}(LyC) measurements from Fletcher et al. (2018) are achieved through SED fitting where $(L_\nu(\mathrm{LyC})/L_\nu(UV))_{int}$ can

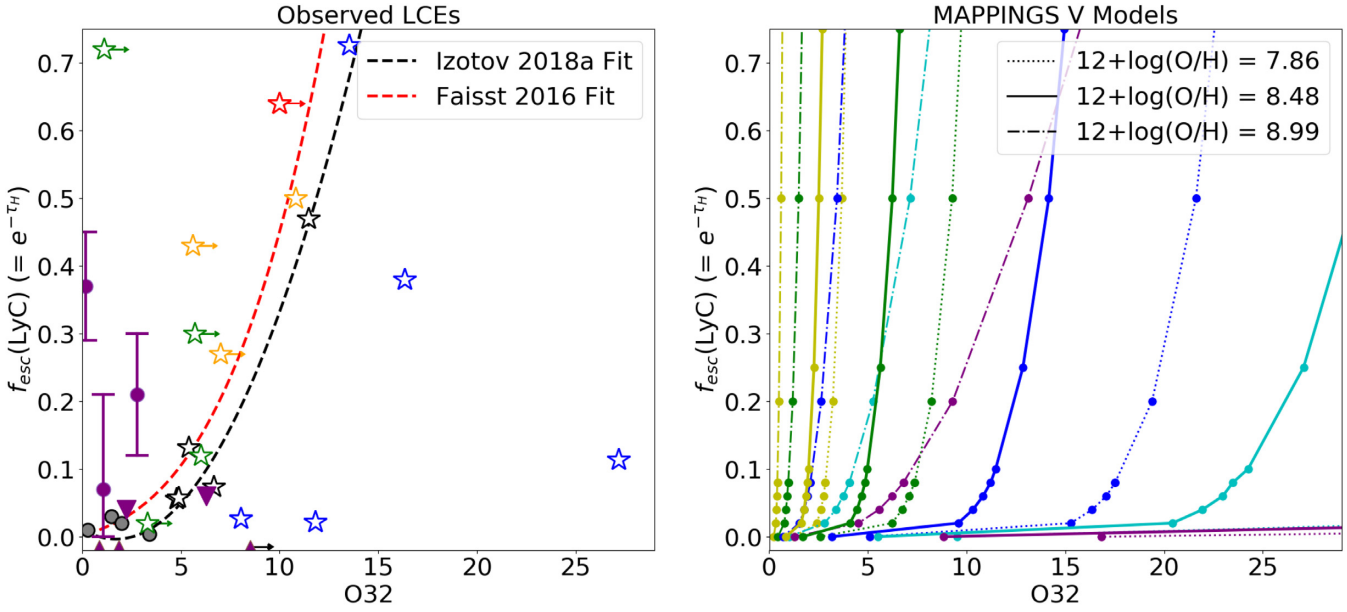

Figure 10. A comparison of the empirical relations between O32 and f_{esc}(LyC) suggested by Izotov et al. (2018b) and Faisst (2016) (left) with the theoretical predictions calculated using MAPPINGS V (right). On the left, LCEs at $z \simeq 0.05$ from Izotov et al. (2016) and Izotov et al. (2018b) are shown as black, open stars as in Figs 6 and LCEs from Izotov et al. (2018a) are shown with blue, open stars. Lower redshift LCEs are indicated with grey circles. The open red star indicates the high redshift LCE, Ion2 (de Barros et al. 2016) and orange and green open stars show 'gold' and 'silver' subsamples of LCEs from the LACES survey (Fletcher et al. 2018). Observations for our sample are shown with purple symbols. Circles with error bars show galaxies with nonzero f_{esc}(LyC) from CLAUDS u-band photometry, downward triangles show upper limits on f_{esc}(LyC) based on CLAUDS u-band uncertainty, and small, upwards triangles show galaxies with f_{esc}(LyC) = 0.0 even when uncertainty in u is considered. The empirical fits presented in Izotov et al. (2018b) and Faisst (2016) and shown by black and red dashed lines, respectively. The fit of Faisst (2016) includes Ion2 and all black LCEs except for the one at the highest O32 and the fit of Izotov et al. (2018b) excludes Ion2 and includes all black, open stars. Blue open stars were reported more recently than either fit, and thus were not included. On the right, coloured lines show the outputs of the MAPPINGS V code at fixed Z with colours indicating different q_{ion}, identical to Fig. 8. Different line styles for MAPPINGS V results correspond to different $12 + log_{10}(O/H)$ as indicated in the legend.

vary from galaxy to galaxy while other LCEs have f_{esc}(LyC) computed assuming a fixed value of 0.33. This should be kept in mind for such a direct comparison as that presented in Fig. 10 as the exact f_{esc}(LyC) likely depend on the computational method.

The empirical fits to LCEs of Faisst (2016) and Izotov et al. (2018b), are shown in the left panel of Fig. 10 using red and black dashed lines, respectively. We note here that Ion2 was not included in the fit of Izotov et al. (2018b) while it was included in the fit of Faisst (2016) (assuming an lower limit of 0.50 on f_{esc}(LyC)). LACES LCEs, as well as the blue, open stars (representing low redshift LCEs of Izotov et al. (2018a)) were reported prior to Faisst (2016) and Izotov et al. (2018b), thus these data are not included in either fit. Interestingly, both empirical fits are qualitatively similar to the MAPPINGS model track for H II regions with $12 + \log_{10}(\mathrm{O/H}) = 8.99$ and $\log_{10}(q_{ion}) = 8.5$ (purple dot-dashed line in right-hand panel of Fig. 10). Galaxies from Izotov et al. (2016) and Izotov et al. (2018b) have measured $12 + \log_{10}(\mathrm{O/H})$ between 7.62 and 8.00, suggesting that this qualitative similarity is merely coincidental. Furthermore, as we have mentioned, the combination of high ionization and high metallicity represented by this track is unlikely for real galaxies.

The most striking discrepancy seen in the left-hand panel of Fig. 10 is that 4/5 of the most recently reported $z \simeq 0.05$ galaxies from Izotov et al. (2018a) have O32 and f_{esc}(LyC) values clearly in disagreement with the earlier fits presented by Faisst (2016) and Izotov et al. (2018b). This discrepancy, which also has been commented on in Izotov et al. (2018a), casts serious doubt on a simple relationship between O32 and f_{esc}(LyC). A similar conclusion has also recently been drawn by Naidu et al. (2018) who find a conspicuous lack of LyC emission from stacked u-band photometry of 73 galaxies at $z = 3.42 - 3.57$ that are inferred to have O32 $\gtrsim 4$.

One possible way to ease the tension in such results is suggested by the MAPPINGS V tracks presented in the right panel of Fig. 10. A more complex relationship between $12 + log_{10}(O/H)$, q_{ion}, and f_{esc}(LyC) may be required (e.g. by including known correlations between metallicity and ionization parameter, Kojima et al. 2017). Confirming this will require a larger sample of LCEs with reliably measured metallicities. Regardless, observations of O32 in confirmed LCEs suggest that all galaxies with f_{esc}(LyC) > 0.20 also have O32 > 10.0. Recent observations of Izotov et al. (2018a) and lower limits on O32 for galaxy 13459 presented here (not detected at LyC wavelengths) clearly show that a large O32 does not require a large observed value of f_{esc}(LyC).

Another possible reason for a discrepancy between O32 vs f_{esc}(LyC) for Izotov et al. (2018a) galaxies and the empirical relationships presented in Faisst (2016) and Izotov et al. (2018b) could be the lack of complex geometry in our photoionization modelling. Observations of individual nearby H II regions show them to be geometrically complex, with significant spatial variation in oxygen line ratios indicative of localised, highly ionized regions from which LyC could escape (e.g. Zastrow et al. 2011; Weilbacher et al. 2015; Kehrig et al. 2016; Keenan et al. 2017; Micheva et al. 2018). Similar regions in high redshift H II regions could represent 'holes" through which LyC flux could escape while other areas of the H II region remain completely opaque to high energy radiation (e.g. models of Zackrisson et al. 2013; Verhamme et al. 2015; Za-

ckrisson et al. 2017). This also highlights a limitation of our density bounded MAPPINGS V photoionization models as these assume homogeneity in $\tau_{H\,I}$, thus a constant f_{esc}(LyC) across the entire nebula. Further discussion of geometric effects on the inferred value of f_{esc}(LyC) can be found in recent works by Steidel et al. (2018) and Fletcher et al. (2018). In particular, Fletcher et al. (2018) point out that the stacking analysis of strong [O III] (λ5007 Å) emitters employed by Naidu et al. (2018) may not provide a reliable average f_{esc}(LyC) where LyC photons escape from H II regions with complex geometry.

To illustrate the geometric effects on observable quantities, we focus on recent observations of LCEs from Izotov et al. (2018a) with extremely high O32 and relatively low f_{esc}(LyC). These observations may be the direct result of differences in geometric dependency as LyC photons must be emitted directly into our line-of-sight while line emission can be scattered into our sight line. High O32 and low f_{esc}(LyC) cases could be explained by a nebular geometry in which dense gas clouds are situated in our line of sight towards the ionizing source, giving a low *observed* f_{esc}(LyC), while a hole (or multiple holes) through the nebula away from our line of sight scatter significant amounts of [O III] line emission towards us. This geometric arrangement is illustrated conceptually on the left side of Fig. 11. Such a case may also highlight an important difference between the *intrinsic* and *observed* values of f_{esc}(LyC), as the latter quantity is highly dependent on $\tau_{H\,I}$ in our direct sight line towards sources of ionizing radiation. This may also suggest that, although recent evidence shows a weak dependence of observed f_{esc}(LyC) and O32, the O32 ratio may indeed correlate with intrinsic f_{esc}(LyC).

Testing this requires full 3D photoionization with radiative transfer and could be performed using existing tools (e.g. Mocassin, Ercolano 2002). Computing even a single modelled H II region in 3D is computationally expensive, thus exploring the parameter space represented by a suite of such models is beyond the scope of the current work. We also note that, particularly in massive galaxies, measured values are marginalised over multiple H II regions within a given galaxy. Exploring 3D models of realistic H II regions (and ensembles of these regions) with regards to LyC escape, however, is an interesting avenue of future research. Given the difficulties highlighted here with respect to O32 other observational signatures expected to probe gas opacity and geometry in H II regions should be explored further both theoretically and observationally. These include high resolution observations of double (or more) peaks in Lyα emission line profiles (e.g. Verhamme et al. 2015; Vanzella et al. 2018), rest-frame UV absorption line optical depths (probing neutral hydrogen covering fractions, e.g. Steidel et al. 2010, 2018; Jones et al. 2013; Leethochawalit et al. 2016), a comparison between Hβ EW and UV spectral slope (providing a direct comparison of photoionization and UV luminosity, e.g. Zackrisson et al. 2013, 2017), or the observation of an empirical relation between $E(B-V)$ and neutral hydrogen covering fraction (Reddy et al. 2016).

Next we comment on the predicted f_{esc}(LyC) for galaxies in our sample based on their measured O32 values as well as the estimated values from Section 4.4 based on CLAUDS u band photometry. The O32 and photometrically estimated f_{esc}(LyC) values of our galaxy sample are indicated in the left-hand panel of Fig. 10 using purple circles with error bars indicating the spread attributable to error in the photometric measurement. Those galaxies with u-band magnitudes consistent with $f_{esc}(\mathrm{LyC}) = 0.0$ are shown along the x-axis using purple triangles. Photometric estimates of f_{esc}(LyC) for 4/8 galaxies in our sample are found to be in agreement, within photometric errors, with the fits of Faisst (2016) and Izotov et al. (2018b). Of the remaining four, our two highest O32 galaxies (16067 and the lower limit for [O II] λλ3727 Å galaxy 13459) both fall below the published relations, similar to Izotov et al. (2018a), while the remaining two are significantly above this relation.

Galaxies falling above the relations of Faisst (2016) and Izotov et al. (2018b) are currently only found in this study and the LACES survey (Fletcher et al. 2018), and of particular interest. We note that from Fletcher et al. (2018) are not detected in [O II] (λλ3727 Å) thus O32 values are lower limits. If such a population of low O32, high f_{esc}(LyC) galaxies is confirmed at $z > 3$, this could suggest an evolution in the ISM properties of high redshift galaxies that more readily allow ionizing photons to escape, even at low q_{ion}. A second alternative is that this is due to a geometric effect in which a galaxy is viewed at a particular line of sight directed at a hole in an H II region directly in line with massive, ionizing stars while the overall covering fraction of dense hydrogen in the nebula is quite high (also discussed in Fletcher et al. 2018). This peculiar geometry is illustrated on the right-hand side of Fig. 11. We reiterate here that a better understanding of the relationship between geometry and f_{esc}(LyC) in 3D, and how this relates to observed quantities in 2D, will likely shed light on the difficulties faced in uncovering a reliable proxy for LyC escape during the EoR.

It is interesting that two of our galaxies falling above the Faisst (2016) and Izotov et al. (2018b) relations in the left-hand panel of Fig. 10, 17251 and 17800, have merger-like HST morphologies seen in Fig. 2. Galaxy 17251 in particular, with the lowest O32 in our sample, has additional evidence of being an on-going merger from the complex [O III] (λ5007 Å) in our 2D spectrum (see Fig. 7). The low O32 (lower limit) LCE from Fletcher et al. (2018) has a low S/N in their HST imaging, thus assessing the possibility of a merger from morphology is not possible. As we have discussed in Sections 5.1.1 and 6.1, shocks associated with mergers can enhance [O II] (λλ3727 Å) relative to [O III] (λ5007 Å), thus explaining to low observed O32 in these galaxies (Rich et al. 2015; Epinat et al. 2018). Observations of these galaxies suggest that galaxy mergers may significantly enhance f_{esc}(LyC), but it is clear that predicting f_{esc}(LyC) for such objects from optical emission lines is complicated due to the presence of shock excitation. Possible mechanisms for an enhanced f_{esc}(LyC) may include redistribution of gas around existing stars or star-formation induced at the outskirts of the merging system where supernova feedback can more easily remove gas from around the newly formed stellar populations.

Finally, we point out that similar galaxies with low O32 and high f_{esc}(LyC) are not present in the low redshift samples of Izotov et al. (2018b) and Izotov et al. (2018a). Green pea galaxies studied at high spatial resolution and with integral field spectroscopy have shown the population to be a mix of merging and non-merging systems (Cardamone et al. 2009; Lofthouse, Houghton & Kaviraj 2017), though the fraction of mergers in green pea samples is still unclear due to low number statistics. Regardless, the merger properties studied in Izotov et al. (2018b) and Izotov et al. (2018a) are not well constrained by current observations. The high O32 for these samples suggests a lack of shock excitation and thus may exclude on-going merger activity, though this does not rule out the possibility they are recent merger remnants. Retrograde mergers are known to funnel gas towards the galaxy centre resulting in compact and intense star formation similar to that seen in green pea samples (e.g. Bassett et al. 2017b). Such a high star formation surface density can enhance feedback and increase the likelihood of LyC escape. A study of LyC emission from confirmed mergers and merger remnants using HST spectroscopy at $z \simeq 0.2 - 0.5$ would help to shed light on the role of mergers in the escape of ionizing radiation.

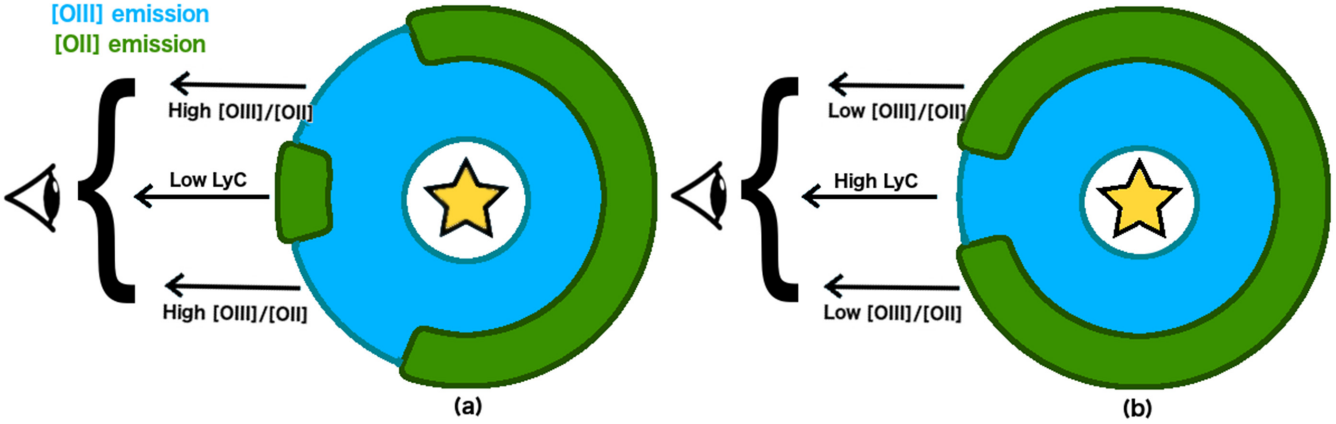

Figure 11. A conceptual picture of the differing geometric effects on observed LyC and scattered line emission from H II regions with holes. Blue indicates the hot, diffuse, [O III] (λ5007 Å) emitting inner regions while green indicates cool, dense, [O II] (λλ3727 Å) emitting outer regions. Giammanco et al. (2005) and Pellegrini et al. (2012), as well as our own MAPPINGS V analysis, have shown that a high gas density results in a lowered observed O32 value. (a): A low overall covering fraction of dense gas with the chance alignment of a small, dense clump that obscures the ionizing photon source(s). This would result in low f_{esc}(LyC) and high O32 (e.g. Izotov et al. 2018a). b: A high overall covering fraction of dense gas with the chance alignment of a small hole in front of the source(s) of ionizing photons. This would result in a high f_{esc}(LyC) and a low O32 (e.g. our sample). See Reddy et al. (2016), Fletcher et al. (2018), and Steidel et al. (2018) for further discussion on the implication of clumpy geometry on f_{esc}(LyC).

7 SUMMARY AND CONCLUSIONS

The long-term goal of our observing program is to provide a method of accurately estimating the level of LyC escape using restframe optical nebular lines where direct LyC detection is not available. An ideal calibration, which is explored in this work, is based on the ratios of bright emission lines as these will be routinely observed from galaxies during the EoR using future observatories (e.g. JWST). LyC emission from galaxies above $z \simeq 6$, on the other hand, will not be observed due to high neutral fraction of the IGM (e.g. Inoue et al. 2014). This means that calibrations based on more readily observable features will be essential in understanding the role of star-forming galaxies in driving reionization.

As a first step toward achieving our goal, we selected eight galaxies at $\langle z \rangle = 3.17$, based on 30 band photometric redshift, with bright *uS* magnitudes, indicative of potential nonzero f_{esc}(LyC). A caveat to our selection is that at $z \sim 3.17$ the *uS* band is contaminated by Ly α forest light. We opted for this redshift range in this pilot survey, however, to minimise the effect of IGM attenuation and to maximise the likelihood of LyC detection. We consider galaxies selected in this way to be candidate Lyman Continuum Emitters (LCEs). These galaxies were observed using MOSFIRE targeting rest-frame optical emission lines and LRIS targeting LyC and Lyα emission. None of these spectral observations showed evidence of contamination from lower redshift galaxies. Bright emission lines from our MOSFIRE observations ([O II] (λλ3727 Å), [O III] (λ4959 Å), [O III] (λ5007 Å), and Hβ), as well as Lyα information from LRIS, were readily detected. We estimate f_{esc}(LyC) from CLAUDS *u* band photometry (Sawicki et al. in preparation). These photometric f_{esc}(LyC) estimates are tentative due to the contribution to *u*-band flux from $\lambda > 912$ Å photons. LyC emission from our LRIS spectroscopy, on the other hand, has required careful analysis, as the signal is faint, resides at short observed wavelengths where the LRIS CCD is less sensitive, and is challenged by ozone lines and difficulty in proper flat-fielding of the data. Improvement of our LRIS data reduction is ongoing and resulting f_{esc}(LyC) from these observations will be the subject of future work (Meštrić et al. in preparation).

Analysis of the emission line properties of the sample provides valuable information regarding the ionization state of the constituent galaxies. This analysis has validated and improved our selection methodology, allowing for more efficient selection of LCEs in subsequent observations. The results of our emission line analysis are as follows:

(i) The O32 ratio, often used as a proxy for ionization parameter, for galaxies in our sample are comparable to other LBG samples at a similar redshift. High O32 galaxies in our sample also overlap with the low O32 end of highly star-forming 'green pea' galaxies at low-redshift, with our highest O32 galaxy having a similar value to known LCEs. The majority of high-redshift LAEs are found to have significantly higher O32 values compared to our sample. Overall, this suggests our sample contains galaxies with ionization parameters typical of the parent population of high-redshift star-forming galaxies but does not include extremely ionized members.

(ii) The ionization parameter is quantified using an iterative calculation (assuming ionization bounded conditions) that estimates $12 + \log_{10}(\mathrm{O/H}) = 8.18 - 8.86$ and $\log_{10}(q_{ion}) = 7.67 - 8.10$ for our sample, comparable to the average for green peas and LBGs presented in Nakajima & Ouchi (2014).

(iii) 5/8 of the galaxies in our sample are also found to be Ly α emitters, and these typically have the highest measured values of O32 among those from our sample (though lower than typical O32 values measured for high redshift LAE samples, e.g. Nakajima et al. 2016).

(iv) We find that photometric observations in the *u*-band (probing LyC at $z \geq 2.9$) are consistent with non-zero LyC escape for 3/8 of the galaxies in our sample (with two additional galaxies having non-zero upper limits). We note that not all galaxies with non-zero f_{esc} estimates also emit Ly α photons.

(v) The two galaxies in our sample with the highest photometric estimates of f_{esc}(LyC) have relatively low O32 and evidence of merger activity. Shocks associated with merging may explain their low observed O32 values.

Difficulties in interpreting f_{esc}(LyC) estimated from u band photometry has informed our selection of future samples to shift to higher redshifts. In doing so, we expect to be able to select a cleaner sample of LCEs as beyond $z = 3.4$ the u band contains only LyC photons. We note that the selection for this pilot survey pre-dates the CLAUDS survey, thus using this new data set allows us to more reliably select LCEs in our on-going work (e.g. Meštrić et al. in preparation).

In addition to the observational results presented above, we also performed 1D photoionization modelling using the MAPPINGS V code to predict the line ratios of H II regions with a variety of nebular conditions. Models explore metallicities in the range $7.86 < 12 + \log_{10}(\mathrm{O/H}) < 8.99$ and ionization parameter in the range $6.5 < \log_{10}(q_{\mathrm{ion}}) < 8.5$. Density bounded models allow us to explore the additional parameter space of f_{esc}(LyC) by varying the optical depth of HI, $\tau_{\mathrm{H\,I}}$. In Section 6.3 we compared our f_{esc}(LyC) models with the empirical relations between O32 and f_{esc}(LyC) proposed by Izotov et al. (2018b) and Faisst (2016) for low-redshift galaxies. The results of this analysis are:

(i) We have shown that the degeneracy between metallicity and ionization on the R23 vs O32 plane also suffers a degeneracy with f_{esc}(LyC), a relevant issue for studies of optical line ratios in LCEs. Density bounded, low metallicity models indicate that, above $f_{esc}(\mathrm{LyC}) = 0.10$, there is little variation in O32 with increasing f_{esc}(LyC). This may hamper the predictive power of this line ratio given the average uncertainties in its measurement at high-redshift.

(ii) The above point, as well as Fig. 10, clearly shows that in order to reasonably estimate f_{esc}(LyC) from optical emission line ratios, an accurate estimate of galaxy metallicity is required. In the future, estimates of galaxy metallicities at $z > 3 - 4$ will be provided using observations of [N II], H α, and [S II] emission lines using JWST with the caveat that these values may also be affected by density bounded conditions in H II regions.

We stress here that photoionization models of MAPPINGS V, as well as the commonly used photoionization code CLOUDY, typically employ homogenous spherical or plane-parallel geometries. Observations of nearby H II regions show extremely complex geometries implying large spatial variation in LyC escape. Full 3D photoionization models, using e.g. the Mocassin code (e.g. Mocassin, Ercolano 2002) in the context of LyC escape will be another interesting avenue of future research that could help to explain peculiar observed pairings of O32 and f_{esc}(LyC) (e.g. Izotov et al. 2018a galaxies with high O32 and low f_{esc}(LyC)). Such simulations will also be instrumental in testing other proposed observational signatures of LyC escape in high redshift galaxies (Steidel et al. 2010; Jones et al. 2013; Zackrisson et al. 2013, 2017; Verhamme et al. 2015; Leethochawalit et al. 2016; Reddy et al. 2016).

The results of this paper further highlight the problems with assuming a simple relationship between O32 and f_{esc}(LyC). Other recent works have explored this issue, focusing on the observation of galaxies with high O32 and low (or zero) f_{esc}(LyC) (e.g. Naidu et al. 2018; Izotov et al. 2018a). A possible explanation for such observations, as mentioned above, is the geometric differences between line emission and LyC observation due to the former being scattered into the line-of-sight. In this work we observe a different type of outliers with low O32 and high f_{esc}(LyC), which we suggest may result from ongoing mergers. Merger activity can both reduce O32 (due to shocks, e.g. Epinat et al. 2018) and redistribute gas and/or induce star formation in the outskirts of the merging system which could enhance f_{esc}(LyC) (see also Bergvall et al. 2013). Current LCE studies may be biased against studying mergers due to selections focusing on compact, isolated galaxies. Although this is typically done at high redshift to avoid line-of-sight contaminants, our results highlight a strong motivation for targeting LyC emission from mergers in future observations. A full understanding of the relationship between O32 and LyC with consideration of merger activity will enable the goal of using these (or similar) nebular lines as proxies for LyC at $z > 6$.

ACKNOWLEDGEMENTS

This research was conducted by the Australian Research Council Centre of Excellence for All Sky Astrophysics in 3 Dimensions (ASTRO 3D), through project number CE170100013. The authors wish to thank E. Zackrisson for useful discussion in the early stages of this work, D. Nicholls for assistance in constructing photoionization models using Modeling And Prediction in PhotoIonized Nebulae and Gasdynamical Shocks (MAPPINGS) V, and the anonymous referee for their comments that have helped to improve the focus, clarity, and relevance of this work. JC acknowledges research support from Australian Research Council Future Fellowship grant FT130101219. TG is grateful to the LABEX Lyon Institute of Origins (ANR-10-LABX-0066) of the Université de Lyon for its financial support within the programme 'Investissements d'Avenir' (ANR-11-IDEX-0007) of the French government operated by the National Research Agency (ANR). (Some of) The data presented herein were obtained at the W. M. Keck Observatory (programs 2015A_W012LA, 2015A_W033M, and 2016A_W034LA), which is operated as a scientific partnership among the California Institute of Technology, the University of California and the National Aeronautics and Space Administration. The Observatory was made possible by the generous financial support of the W. M. Keck Foundation. The authors wish to recognize and acknowledge the very significant cultural role and reverence that the summit of Maunakea has always had within the indigenous Hawaiian community. We are most fortunate to have the opportunity to conduct observations from this mountain.

REFERENCES

Alexandroff R. M., Heckman T. M., Borthakur S., Overzier R., Leitherer C., 2015, ApJ, 810, 104
Allen M. G., Groves B. A., Dopita M. A., Sutherland R. S., Kewley L. J., 2008, ApJS, 178, 20
Bassett R. et al., 2017a, MNRAS, 467, 239
Bassett R., Bekki K., Cortese L., Couch W., 2017b, MNRAS, 471, 1892
Becker G. D., Bolton J. S., Madau P., Pettini M., Ryan-Weber E. V., Venemans B. P., 2015, MNRAS, 447, 3402
Bergvall N., Leitet E., Zackrisson E., Marquart T., 2013, A&A, 554, A38
Bian F., Fan X., McGreer I., Cai Z., Jiang L., 2017, ApJ, 837, L12
Borthakur S., Heckman T. M., Leitherer C., Overzier R. A., 2014, Science, 346, 216
Bouwens R. J., Illingworth G. D., Oesch P. A., Caruana J., Holwerda B., Smit R., Wilkins S., 2015, ApJ, 811, 140
Bouwens R. J., Smit R., Labbé I., Franx M., Caruana J., Oesch P., Stefanon M., Rasappu N., 2016, ApJ, 831, 176
Bouwens R. J., Illingworth G. D., Oesch P. A., Atek H., Lam D., Stefanon M., 2017, ApJ, 843, 41
Calzetti D., Kinney A. L., Storchi-Bergmann T., 1994, ApJ, 429, 582
Calzetti D., Armus L., Bohlin R. C., Kinney A. L., Koornneef J., Storchi-Bergmann T., 2000, ApJ, 533, 682
Cardamone C. et al., 2009, MNRAS, 399, 1191
Cardelli J. A., Clayton G. C., Mathis J. S., 1989, ApJ, 345, 245
Chabrier G., 2003, PASP, 115, 763

Chevallard J. et al., 2018, MNRAS, 479, 3264
Chisholm J., Orlitová I., Schaerer D., Verhamme A., Worseck G., Izotov Y. I., Thuan T. X., Guseva N. G., 2017, A&A, 605, A67
Cooke J., Ryan-Weber E. V., Garel T., Díaz C. G., 2014, MNRAS, 441, 837
Cowley M. J. et al., 2016, MNRAS, 457, 629
de Barros S. et al., 2016, A&A, 585, A51
Dopita M. A. et al., 2006, ApJS, 167, 177
Dressler A., Henry A., Martin C. L., Sawicki M., McCarthy P., Villaneuva E., 2015, ApJ, 806, 19
Eldridge J. J., Stanway E. R., Xiao L., McClelland L. A. S., Taylor G., Ng M., Greis S. M. L., Bray J. C., 2017, PASA, 34, e058
Elmegreen D. M., Elmegreen B. G., Rubin D. S., Schaffer M. A., 2005, ApJ, 631, 85
Epinat B. et al., 2018, A&A, 609, A40
Erb D. K., Steidel C. C., Shapley A. E., Pettini M., Reddy N. A., Adelberger K. L., 2006, ApJ, 647, 128
Ercolano B., 2002, PhD thesis, University of London, University College London (United Kingdom)
Faisst A. L., 2016, ApJ, 829, 99
Fan X., Carilli C. L., Keating B., 2006, ARA&A, 44, 415
Fletcher T. J., Robertson B. E., Nakajima K., Ellis R. S., Stark D. P., Inoue A., 2018, preprint (arXiv:1806.01741)
Fontanot F., Cristiani S., Vanzella E., 2012, MNRAS, 425, 1413
Forrest B. et al., 2017, ApJ, 838, L12
Förster Schreiber N. M., Shapley A. E., Erb D. K., Genzel R., Steidel C. C., Bouché N., Cresci G., Davies R., 2011, ApJ, 731, 65
Garn T., Best P. N., 2010, MNRAS, 409, 421
Giammanco C., Beckman J. E., Cedrés B., 2005, A&A, 438, 599
Gordon K. D., Clayton G. C., 1998, ApJ, 500, 816
Grazian A. et al., 2016, A&A, 585, A48
Hassan S., Davé R., Mitra S., Finlator K., Ciardi B., Santos M. G., 2018, MNRAS, 473, 227
Heckman T. M. et al., 2011, ApJ, 730, 5
Hopkins P. F., Richards G. T., Hernquist L., 2007, ApJ, 654, 731
Inoue A. K., Iwata I., Deharveng J.-M., Buat V., Burgarella D., 2005, A&A, 435, 471
Inoue A. K., Shimizu I., Iwata I., Tanaka M., 2014, MNRAS, 442, 1805
Izotov Y. I., Schaerer D., Thuan T. X., Worseck G., Guseva N. G., Orlitová I., Verhamme A., 2016, MNRAS, 461, 3683
Izotov Y. I., Guseva N. G., Fricke K. J., Henkel C., Schaerer D., 2017, MNRAS, 467, 4118
Izotov Y. I., Worseck G., Schaerer D., Guseva N. G., Thuan T. X., Fricke K. J., Verhamme A., Orlitová I., 2018a, MNRAS , 478, 4851
Izotov Y. I., Schaerer D., Worseck G., Guseva N. G., Thuan T. X., Verhamme A., Orlitová I., Fricke K. J., 2018b, MNRAS, 474, 4514
Jaskot A. E., Oey M. S., 2013, ApJ, 766, 91
Jiang L. et al., 2008, AJ, 135, 1057
Jones T. A., Ellis R. S., Schenker M. A., Stark D. P., 2013, ApJ, 779, 52
Kashino D. et al., 2013, ApJ, 777, L8
Keenan R. P., Oey M. S., Jaskot A. E., James B. L., 2017, ApJ, 848, 12
Kehrig C. et al., 2016, MNRAS, 459, 2992
Kelson D. D., 2003, PASP, 115, 688
Kennicutt R. C., Evans N. J., 2012, ARA&A, 50, 531
Kewley L. J., Dopita M. A., 2002, ApJS, 142, 35
Kojima T., Ouchi M., Nakajima K., Shibuya T., Harikane Y., Ono Y., 2017, PASJ, 69, 44
Komatsu E. et al., 2011, ApJS, 192, 18
Lange R. et al., 2015, MNRAS, 447, 2603
Leethochawalit N., Jones T. A., Ellis R. S., Stark D. P., Zitrin A., 2016, ApJ, 831, 152
Leitet E., Bergvall N., Hayes M., Linné S., Zackrisson E., 2013, A&A, 553, A106
Leitherer C. et al., 1999, ApJS, 123, 3
Leitherer C., Hernandez S., Lee J. C., Oey M. S., 2016, ApJ, 823, 64
Lofthouse E. K., Houghton R. C. W., Kaviraj S., 2017, MNRAS, 471, 2311
Maiolino R. et al., 2008, A&A, 488, 463
Martín-Manjón M. L., García-Vargas M. L., Mollá M., Díaz A. I., 2010, MNRAS, 403, 2012
Masters D. et al., 2012, ApJ, 755, 169
Matthee J., Sobral D., Best P., Khostovan A. A., Oteo I., Bouwens R., Röttgering H., 2017, MNRAS, 465, 3637
McGreer I. D., Fan X., Jiang L., Cai Z., 2018, ApJ, 155, 131
Meurer G. R., Heckman T. M., Calzetti D., 1999, ApJ, 521, 64
Micheva G., Oey M. S., Keenan R. P., Jaskot A. E., James B. L., 2018, ApJ, 867, 2
Mitra S., Ferrara A., Choudhury T. R., 2013, MNRAS, 428, L1
Nagao T., Maiolino R., Marconi A., 2006, A&A, 459, 85
Naidu R. P., Forrest B., Oesch P. A., Tran K.-V. H., Holden B. P., 2018, MNRAS , 478, 791, 478, 791
Nakajima K., Ouchi M., 2014, MNRAS, 442, 900
Nakajima K., Ellis R. S., Iwata I., Inoue A. K., Kusakabe H., Ouchi M., Robertson B. E., 2016, ApJ, 831, L9
Nanayakkara T. et al., 2016, ApJ, 828, 21
Nestor D. B., Shapley A. E., Steidel C. C., Siana B., 2011, ApJ, 736, 18
Nicholls D. C., Sutherland R. S., Dopita M. A., Kewley L. J., Groves B. A., 2017, MNRAS, 466, 4403
Oke J. B., Postman M., Lubin L. M., 1998, AJ, 116, 549
Onodera M. et al., 2016, ApJ, 822, 42
Osterbrock D. E., 1989, Astrophysics of gaseous nebulae and active galactic nuclei, University Science Books, Sausalito, CA
Ouchi M. et al., 2009, ApJ, 706, 1136
Paardekooper J.-P., Khochfar S., Dalla Vecchia C., 2015, MNRAS, 451, 2544
Pagel B. E. J., Edmunds M. G., Blackwell D. E., Chun M. S., Smith G., 1979, MNRAS, 189, 95
Pellegrini E. W., Oey M. S., Winkler P. F., Points S. D., Smith R. C., Jaskot A. E., Zastrow J., 2012, ApJ, 755, 40
Raičević M., Theuns T., Lacey C., 2011, MNRAS, 410, 775
Rauw G. et al., 2015, ApJS, 221, 1
Reddy N. A. et al., 2015, ApJ, 806, 259
Reddy N. A. et al., 2018, ApJ, 853, 56
Reddy N. A., Erb D. K., Pettini M., Steidel C. C., Shapley A. E., 2010, ApJ, 712, 1070
Reddy N. A., Steidel C. C., Pettini M., Bogosavljević M., Shapley A. E., 2016, ApJ, 828, 108
Rich J. A., Kewley L. J., Dopita M. A., 2015, ApJS, 221, 28
Robertson B. E. et al., 2013, ApJ, 768, 71
Rosdahl J. et al., 2018, MNRAS, 479, 994
Salpeter E. E., 1955, ApJ, 121, 161
Sanders R. L. et al., 2016, ApJ, 825, L23
Scoville N. et al., 2007, ApJS, 172, 1
Shapley A. E., Steidel C. C., Pettini M., Adelberger K. L., 2003, ApJ, 588, 65
Shapley A. E., Steidel C. C., Pettini M., Adelberger K. L., Erb D. K., 2006, ApJ, 651, 688
Shapley A. E., Steidel C. C., Strom A. L., Bogosavljević M., Reddy N. A., Siana B., Mostardi R. E., Rudie G. C., 2016, ApJ, 826, L24
Shivaei I. et al., 2018, ApJ, 855, 42
Shull J. M., Stevans M., Danforth C. W., 2012, ApJ, 752, 162
Siana B. et al., 2007, ApJ, 668, 62
Skrutskie M. F. et al., 2006, AJ, 131, 1163
Speagle J. S., Steinhardt C. L., Capak P. L., Silverman J. D., 2014, ApJS, 214, 15
Spitler L. R. et al., 2014, ApJ, 787, L36
Stark D. P. et al., 2015, MNRAS, 454, 1393
Stark D. P. et al., 2017, MNRAS, 464, 469
Steidel C. C. et al., 2014, ApJ, 795, 165
Steidel C. C., Giavalisco M., Pettini M., Dickinson M., Adelberger K. L., 1996, ApJ, 462, L17
Steidel C. C., Pettini M., Adelberger K. L., 2001, ApJ, 546, 665
Steidel C. C., Shapley A. E., Pettini M., Adelberger K. L., Erb D. K., Reddy N. A., Hunt M. P., 2004, ApJ, 604, 534
Steidel C. C., Erb D. K., Shapley A. E., Pettini M., Reddy N., Bogosavljević M., Rudie G. C., Rakic O., 2010, ApJ, 717, 289
Steidel C. C., Strom A. L., Pettini M., Rudie G. C., Reddy N. A., Trainor R. F., 2016, ApJ, 826, 159

Steidel C. C., Bogosavlevic M., Shapley A. E., Reddy N. A., Rudie G. C., Pettini M., Trainor R. F., Strom A. L., 2018, preprint (arXiv:1805.06071)
Storey P. J., Hummer D. G., 1995, MNRAS, 272, 41
Straatman C. M. S. et al., 2016, ApJ, 830, 51
Swinbank A. M. et al., 2011, ApJ, 742, 11
Tomczak A. R. et al., 2016, ApJ, 817, 118
Trebitsch M., Blaizot J., Rosdahl J., Devriendt J., Slyz A., 2017, MNRAS, 470, 224
Troncoso P. et al., 2014, A&A, 563, A58
Ueda Y., Akiyama M., Hasinger G., Miyaji T., Watson M. G., 2014, ApJ, 786, 104
Vanzella E. et al., 2012, ApJ, 751, 70
Vanzella E. et al., 2015, A&A, 576, A116
Vanzella E. et al., 2016, ApJ, 825, 41
Vanzella E. et al., 2018, MNRAS, 476, 15
Vanzella E. et al., 2018, MNRAS, 476, L15
Vanzella E., Siana B., Cristiani S., Nonino M., 2010, MNRAS, 404, 1672
Verhamme A., Orlitová I., Schaerer D., Hayes M., 2015, A&A, 578, A7
Verhamme A., Orlitová I., Schaerer D., Izotov Y., Worseck G., Thuan T. X., Guseva N., 2017, A&A, 597, A13
Weilbacher P. M. et al., 2015, A&A, 582, A114
Wise J. H., Cen R., 2009, ApJ, 693, 984
Wise J. H., Demchenko V. G., Halicek M. T., Norman M. L., Turk M. J., Abel T., Smith B. D., 2014, MNRAS, 442, 2560
Wisnioski E., Glazebrook K., Blake C., Poole G. B., Green A. W., Wyder T., Martin C., 2012, MNRAS, 422, 3339
Yajima H., Choi J.-H., Nagamine K., 2011, MNRAS, 412, 411
Yang H., Malhotra S., Gronke M., Rhoads J. E., Dijkstra M., Jaskot A., Zheng Z., Wang J., 2016, ApJ, 820, 130
Zackrisson E. et al., 2017, ApJ, 836, 78
Zackrisson E., Inoue A. K., Jensen H., 2013, ApJ, 777, 39
Zahid H. J., Yates R. M., Kewley L. J., Kudritzki R. P., 2013, ApJ, 763, 92
Zahn O. et al., 2012, ApJ, 756, 65
Zastrow J., Oey M. S., Veilleux S., McDonald M., Martin C. L., 2011, ApJ, 741, L17

This paper has been typeset from a TEX/LATEX file prepared by the author.